รายงานวิจัยฉบับสมบูรณ์

โครงการการศึกษากลไกปฏิกิริยาของเอนไซม์ 3-ไฮดรอกซีเบนโซเอต 6-ไฮดรอกซีเลส จากเชื้อโรโดคอคคัสจอสติไอ

Mechanistic studies of 3-hydroxybenzoate 6-hydroxylase from *Rhodoccocus jostii* RHA1

โดย ผู้ช่วยศาสตราจารย์ ดร. ทันตแพทย์ จีรัสย์ สุจริตกุล

เดือน ปี ที่เสร็จโครงการ ๑๖ กรกฎาคม ๒๕๕๘

สัญญาเลขที่ RSA5580050

รายงานวิจัยฉบับสมบูรณ์

โครงการการศึกษากลไกปฏิกิริยาของเอนไซม์ 3-ไฮดรอกซีเบนโซเอต 6-ไฮดรอกซีเลส จากเชื้อโรโดคอคคัสจอสติไอ

Mechanistic studies of 3-hydroxybenzoate 6-hydroxylase from *Rhodoccocus jostii* RHA1

ผู้วิจัย ผู้ช่วยศาสตราจารย์ ดร. ทันตแพทย์ จีรัสย์ สุจริตกุล
สังกัด ภาควิชาชีวเคมี คณะทันตแพทยศาสตร์ จุฬาลงกรณ์มหาวิทยาลัย

สนับสนุนโดยสำนักงานกองทุนสนับสนุนการวิจัย
และจุฬาลงกรณ์มหาวิทยาลัย

กิตติกรรมประกาศ

ในส่วนของผลงานวิจัยที่สำเร็จลุล่วงแล้ว ผู้วิจัยขอขอบพระคุณ กองทุนรัชดาภิเษกสมโภช จุฬาลงกรณ์มหาวิทยาลัย คณะทันตแพทยศาสตร์ จุฬาลงกรณ์มหาวิทยาลัย ในการให้การสนับสนุนทางด้านการเงิน และเจ้าหน้าที่ของสำนักงานกองทุนสนับสนุนการวิจัยทุกท่านที่ช่วยดำเนินการสนับสนุนทางด้านเอกสารรวมทั้งคำปรึกษา

ผู้วิจัยขอขอบพระคุณ ศาสตราจารย์ ดร. พิมพ์ใจ ใจเย็น ในส่วนของการให้คำปรึกษาในงานวิจัยที่เป็นประโยชน์เสมอมาและสนับสนุนการใช้เครื่องมือ stopped-flow spectrometer ซึ่งเป็นเครื่องมือที่สำคัญในงานวิจัย รวมทั้งแก้ไขการเขียนบทความ นอกจากนี้รวมถึงสมาชิกในห้องปฏิบัติการที่ช่วยสละเวลาในการดูแลเครื่องมือให้อยู่สภาพพร้อมใช้งาน

ผู้วิจัยขอขอบพระคุณ Prof. Dr. William van Berkel ในการสนับสนุนเกี่ยวกับข้อมูลโครงสร้างสามมิติของเอนไซม์ที่ใช้ในการศึกษาครั้งนี้ รวมทั้งแก้ไขการเขียนบทความ

ผู้วิจัยขอขอบพระคุณ Prof. Dr. Barry Entsch ที่ช่วยกรุณาอ่านและแก้ไขข้อบกพร่องในการเขียนบทความ

Abstract

Project Code: RSA5580050

Project Title: Mechanistic studies of 3-hydroxybenzoate 6-hydroxylase from *Rhodoccocus jostii* RHA1

Jeerus Sucharitakul, Department of Biochemistry, Faculty of Dentistry, Chulalongkorn University

E-mail address: Jeerus.s@chula.ac.th

Project Period: 16 July 2012-16 July 2015

Hydroxybenzoate 6-hydroxylase (3HB6H) from *Rhodococcus jostii* RHA1 is an NADH-specific flavoprotein monooxygenase containing flavin adenine dinucleotide (FAD) as a cofactor. The enzyme catalyzes para-hydroxylation of 3-hydroxybenzoate (3 HB) to form 2,5-dihydroxybenzoate (2,5-DHB). The enzyme reaction mechanism was studied using stopped-flow spectrophotometry and rapid-quench techniques. The overall catalytic reaction consists of two half-reactions. The reductive half-reaction is the reduction of FAD by NADH and an oxidative half-reaction is the hydroxylation of the aromatic substrate. Kinetics of enzyme reduction has indicated that 3-HB act as an effector that can increase the reduction rate constant dramatically ~119-fold (0.43 s^{-1} in the absence of 3-HB versus 51 s^{-1} in the presence of 3-HB). For the oxidative half-reaction, the reduced enzyme-3HB complex reacts with oxygen to form two intermediates. The first intermediate is C(4a)-peroxyflavin, which forms with a rate constant of $1.13 \pm 0.01 \times 10^{6}$ $M^{-1} s^{-1}$, while the second intermediate is C(4a)-hydroperoxyflavin. The second intermediate formed with a slower rate constant in D_2O with a SKIE of 1.76, indicating that this step is involved with proton transfer. The hydroxylation occurs with the rate constant of 35 ± 2 s^{-1} and 86% of the product formation. The correlation between pre-steady state and steady-state kinetics indicates that the steps of product release (~12 s^{-1}) and hydroxylation partially control the overall catalytic turnover.
Based on the enzyme crystal structure, the residues H213 and Y217 potentially interact with 3-OH and carbonyl oxygen of 3-HB, respectively. Site-directed mutagenesis of these two residues are employed to investigate their functional roles. The H213A variant can form C4a-hydroperoxyflavin but cannot hydroxylate 3-HB. Both hydroxylation rate constant (1.6 ± 0.02 s^{-1}) and percentage of product formation (25%) of the H213S variant are less than those of the wild-type enzyme. Interestingly, the hydroxylation rate constant of H213E (35 s^{-1}) is similar to the value of wild-type enzyme and the variant is more efficient in hydroxylation (~ 92% product formation). Studies of Y217 variants, Y217A, Y217F and Y217S, indicate that these enzymes cannot bind 3-HB well. The results indicate that H213 is important for hydroxylation while Y217 is necessary for substrate binding.

Keywords: Flavin, Flavin adenine dinucleotide (FAD), Flavoprotein hydroxylase, 3HB6H, 3-hydroxybenzoate 6-hydroxylase, 3HB, 3-hydroxybenzoate, para-hydroxylation, transient kinetics, rapid kinetics, pre-steady state kinetics

บทคัดย่อ

สัญญาเลขที่: RSA5580050

ชื่อโครงการ: โครงการการศึกษากลไกปฏิกิริยาของเอนไซม์ 3-ไฮดรอกซีเบนโซเอต 6-ไฮดรอกซีเลสจากเชื้อโรโดคอคคัสจอสติไอ

จีรัสย์ สุจริตกุล, Department of Biochemistry, Faculty of Dentistry, Chulalongkorn University

E-mail address: Jeerus.s@chula.ac.th

ระยะเวลา: ๑๖ กรกฎาคม ๒๕๕๕ ถึงวันที่ ๑๖ กรกฎาคม ๒๕๕๘

เอนไซม์ 3-ไฮดรอกซีเบนโซเอต 6- ไฮดรอกซีเลส (3HB6H) จากเชื้อโรโคคอคคัส เป็นเอนไซม์ที่เร่งปฏิกิริยาการเกิดไฮดรอกซีเลชันของสับสเตรท 3-ไฮดรอกซีเบนโซเอต (3HB) ได้สารผลิตภัณฑ์เป็น 2,5 ไดไฮดรอกซีเบนโซเอต (2,5-DHB) เอนไซม์ดังกล่าวจัดอยู่ในกลุ่มฟลาโวโปรตีนซึ่งมี ฟลาวินอะดีนินไดนิวคลีโอไทด์ (FAD) เป็นโคแฟคเตอร์ ในงานวิจัยนี้เป็นการศึกษากลไกปฏิกิริยาของเอนไซม์ในระดับ pre-steady state kinetic ซึ่งใช้เครื่องมือที่เรียกว่า stopped-flow spectrometer เพื่อวัดสารตัวกลางที่เกิดขึ้นและสลายอย่างรวดเร็วระหว่างการเกิดปฏิกิริยา ปฏิกิริยาของเอนไซม์ประกอบด้วย 2 ส่วน ส่วนแรกเรียกว่า รีดักทีฟฮาร์ฟรีแอคชัน เกิดจากนิโคตินาไมด์อะดีนินไดนิวคลีโอไทด์ (NADH) ซึ่งเป็นสับสเตรทของจะให้อิเลคตรอนแก่เอนไซม์ โดย FAD โคแฟคเตอร์ของเอนไซม์จะป็นตัวรับอิเลคตรอน ผลการทดลองพบว่าเมื่อมี 3HB จะช่วยเร่งการเกิดปฏิกิริยาให้เร็วขึ้นประมาณ 119 เท่า (จาก 0.435 s^{-1} เป็น 51 s^{-1}) ส่วนอีกปฏิกิริยาเรียกว่า ออกซิเดทีฟฮาร์ฟรีแอคชัน เกิดจากรีดิวน์เอนไซม์จากขั้นแรกทำปฏิกิริยากับออกซิเจนและเกิดเป็นสารตัวกลางเรียกว่า C4a-hydroperoxyflavin ด้วยค่าคงที่อัตราเร็วปฏิกิริยาเท่ากับ $1.13 \pm 0.01 \times 10^6$ $M^{-1}s^{-1}$ และสารตัวกลางดังกล่าวทำให้เกิดปฏิกิริยาไฮดรอกซีเลชันของสับสเตรท ด้วยค่าคงที่อัตราเร็วปฏิกิริยาเท่ากับ 35 ± 2 s^{-1} และเกิดสารผลิตภัณฑ์ประมาณ 80% เมื่อเทียบกับความเข้มข้นตั้งต้นของเอนไซม์ จากข้อมูลโครงสร้างโมเลกุลสามมิติของเอนไซม์พบว่ากรดอะมิโน H213 สามารถเกิดพันธะไฮโดรเจนกับหมู่ฟังชันก์ 3-ไฮดรอกซีของสับสเตรท และกรดอะมิโน Y217 สามารถพันธะไฮโดรเจนกับหมู่ฟังชันก์คาร์บอกซิลิคของสับสเตรท เมื่อเปลี่ยนกรดอะมิโน H213 ไปเป็น alanine ทำให้เอนไซม์ไม่สามารถสร้างสารผลิตภัณฑ์ได้ ในขณะที่เปลี่ยนไปเป็น aspartate และ serine กลับสร้างสารผลิตภัณฑ์ได้ลดลง แต่เมื่อเปลี่ยนเป็น glutamate กลับสร้างสารผลิตภัณฑ์ได้มากกว่า wild type เอนไซม์เป็น 92% แสดงว่ากรดอะมิโนดังดล่าวสำคัญต่อการเกิดปฏิกิริยาไฮดรอกซีเลชัน เมื่อเปลี่ยนกรดอะมิโน Y217 ไปเป็น alanine serine phenylalanine พบว่าเอนไซม์ไม่สามารถจับกับสับสเตรท แสดงว่ากรดอะมิโนดังดล่าวสำคัญต่อการจับกับสับสเตรท

คำสำคัญ: Flavin, Flavin adenine dinucleotide (FAD), Flavoprotein hydroxylase, 3HB6H, 3-hydroxybenzoate 6-hydroxylase, 3HB, 3-hydroxybenzoate, para-hydroxylation, transient kinetics, rapid kinetics, pre-steady state kinetics

The Reaction Kinetics of 3-Hydroxybenzoate 6-Hydroxylase from *Rhodoccocus jostii* RHA1 Provide an Understanding of the para-Hydroxylation Enzyme Catalytic Cycle

Monooxygenases or hydroxylases are useful biocatalysts for catalyzing regio-specific oxygenation by molecular oxygen under mild conditions. Many hydroxylation reactions of aromatic compounds found in nature are carried out by flavin-dependent enzymes that belong to the class of external flavoprotein monooxygenases that require NADH or NADPH as an external reductant (1-3). The overall reaction of these enzymes can be divided into a reductive half-reaction, in which two electrons are transferred from NAD(P)H to the enzyme-bound flavin, and an oxidative half-reaction in which the hydroxylation of aromatic substrate takes place. The overall reaction can be carried out within a single polypeptide (designated as Class A monooxygenases in (1)) or by two-protein components (designated as Class D monooxygenases in (1). The current knowledge obtained from studying monooxygenases that catalyze *ortho*-hydroxylation reactions support a model in which a flavin adduct intermediate (C4a-hydroperoxyflavin) participates as an electrophile in the electrophilic aromatic substitution reaction to give a C4a-hydroxyflavin and a hydroxylated product (4-9). The best understood enzyme of this class is *p*-hydroxybenzoate 3-hydroxylase (PHBH), for which detailed studies on the enzyme structure and kinetics have revealed a great deal of complexity in the protein dynamics (3).

3-Hydroxybenzoate 6-hydroxylase (3HB6H) is one of the flavin-dependent enzymes that have been reported to catalyze *para*-hydroxylation of aromatic compounds (10). These *para*-hydroxylation enzymes are involved in the degradation pathways of phenolic compounds by bacteria (1, 11) or the biosynthetic pathways of antibiotics such as angucyclines and rhodomycin (12, 13). 3HB6H from *Rhodococcus jostii* RHA1 catalyzes the *para*-hydroxylation of 3-hydroxybenzoate to yield 2,5-dihydroxybenzoate (Figure 1). The enzyme was cloned and expressed in *E. coli*, and was shown to be a dimeric protein containing one FAD per 47 kDa subunit (10). The catalytic reaction of 3HB6H consists of two half-reactions similar to other single-component flavoprotein hydroxylases. Investigation on the kinetics of the reductive half-reaction has demonstrated that when bound to the enzyme, substrate and product act as effectors to increase the rate of flavin reduction by two orders of magnitude (14). It was also shown that 3HB6H catalyzes the regio-specific *para*-hydroxylation of a number of 3-hydroxybenzoate analogs (10). Therefore, 3HB6H is potentially useful for synthesizing gentisate compounds that are drugs or antioxidants (15, 16). Recently, the crystal structures of the wild-type and mutant 3HB6H enzymes

were solved (17). Although the overall structure of 3HB6H is similar to other single-component flavoprotein aromatic hydroxylases, the arrangement of the active site residues is quite different from other *ortho*-hydroxylation enzymes such as PHBH. The difference in active site environment is presumably important for the regio-specific *para*-hydroxylation process (17).

Up to now, there have been no reports on the kinetic mechanisms related to the overall catalytic cycle of a *para*-hydroxylation flavoenzyme. Therefore, we set out to investigate the kinetics of the oxidative half-reaction of 3HB6H from *R. jostii* RHA1 using stopped-flow and rapid-quench flow techniques. Solvent kinetic isotope effects were used to identify the steps that involved proton transfer. The results provide an understanding of the oxygenation mechanism of 3HB6H and reveal different catalytic features between *para*- and *ortho*-hydroxylating flavoenzymes.

EXPERIMENTAL PROCEDURES

Reagents. NADH (purity $\geq$ 95%) and FAD (purity $\geq$ 95%) were purchased from Sigma-Aldrich. 3-Hydroxybenzoic acid (3HB) and 2,5-dihydroxybenzoic acid (2,5-DHB) were purchased from Merck. The concentrations of compounds were determined using the following absorption coefficients at pH 8.0; NADH, ε_{340} = 6.22 $\times$ 10^3 $M^{-1}cm^{-1}$; FAD, ε_{450} = 11.3 $\times$ 10^3 $M^{-1}cm^{-1}$; 3HB, ε_{288} = 2.0 $\times$ 10^3 $M^{-1}cm^{-1}$; 2,5-DHB, ε_{320} = 4.1 $\times$ 10^3 $M^{-1}cm^{-1}$. All of the absorption coefficient values are for the compounds in solution at pH 8.0. 3HB6H was purified according to the protocol previously described (14). Concentrations of the enzyme were determined using the known absorption coefficient ε_{452} = 11.00 $\pm$ 0.03 $\times$ 10^3 $M^{-1}cm^{-1}$ (one FAD per subunit) (14).

Spectroscopic Studies. UV-visible absorbance spectra were recorded using a Hewlett-Packard diode array spectrophotometer (HP8453), a Shimadzu 2501PC spectrophotometer or a Cary 300Bio double-beam spectrophotometer at 25 $^{\circ}$C. All spectrophotometers were equipped with thermostated cell compartments. Typical assays contained 10 mM 3HB, 2 μM FAD and 1 mM NADH. As this concentration of NADH would give absorbance of ~6 at 340 nm, we thus measured the decrease in absorbance at 395 nm (ε_{395} of 0.22 $\times$ 10^3 $M^{-1}cm^{-1}$), which still gives good linearity for enzyme assays.

Steady-state kinetics. To determine an apparent catalytic constant (k_{cat}) at 4 $^{\circ}$C, a solution of the enzyme at 1 μM in the presence of 10 mM 3HB and 2 μM FAD in air saturation (0.26 mM oxygen) was mixed with an oxygenated buffer (1.92 mM oxygen) plus 10 mM 3HB, 10 mM NADH

and 2 μM FAD using a stopped-flow spectrometer. Final concentrations of the reagents after mixing were 0.5 μM enzyme, 10 mM 3HB, 5 mM NADH and 1.09 mM oxygen. The apparent k_{cat} from steady-state experiments was compared to the value calculated based on Equation 1 and individual rate constants obtained from rapid-kinetics experiments. Derivations of Equation 1 were carried out according to the method described by Cha (18) and Cramer's rule (19) (see derivations in Supplemental Information)

$$\frac{e}{v} = \frac{1}{\frac{k_3 k_4 [3HB][NADH]}{K_d^1 K_d^2 + K_d^2[3HB] + [3HB][NADH]} + k_6(k_{-3} + k_4)} \times \left[\left(\frac{k_{-5} k_4 k_3 [3HB][NADH]}{k_5 k_7 k_8 [O_2](K_d^1 K_d^2 + K_d^2[3HB] + [3HB][NADH])} + k_6 \left(\frac{k_{-5}}{k_5 k_7 k_8 [O_2]} + \frac{1}{k_5 k_8} \right)(k_{-3} + k_4) \right)(k_8 + k_{10}) + (k_8 + k_{10}) \left(\frac{k_6(k_{-3} + k_4)}{k_7 k_8 [O_2]} + \frac{(k_{-3} + k_4)}{k_8} + \frac{k_3 [3HB][NADH]}{K_d^1 K_d^2 + K_d^2[3HB] + [3HB][NADH]} \times \left(\frac{k_4}{k_7 k_8 [O_2]} + \frac{1}{k_8} \right) \right) \right] + \frac{1}{k_{12}} + \frac{1}{k_{11}} + \frac{1}{k_9} + \frac{1}{k_8} \quad (1)$$

Rapid Reaction Experiments. Reactions were carried out in 100 mM Tris-H_2SO_4 pH 8.0, 4 ºC, unless otherwise specified. The measurements were performed using a TgK Scientific Model SF-61DX or a TgK Scientific Model SHU-61SX2 stopped-flow spectrophotometer in single-mixing mode. The stopped-flow apparatus was made anaerobic by flushing the flow system with an anaerobic buffer solution containing 0.5 mg/ml dithionite in 100 mM sodium phosphate pH 7.0, and equilibrated in the dithionite solution overnight. The flow system of the stopped-flow instrument was washed with anaerobic 100 mM Tris-H_2SO_4 pH 8.0 for three times before starting the experiments.

For preparation of a reduced enzyme solution, an anaerobic oxidized enzyme solution was placed in a tonometer and reduced with an equivalent amount of dithionite (0.2 mg/ml in 100 mM Tris-H_2SO_4 pH 8.0), which was delivered from a gas-tight syringe with a microtitrator attached to the tonometer. The enzyme reduction was monitored through a cuvette attached to the tonometer to ensure a stoichiometric reduction process (20). The reduced enzyme solution was mixed with buffers containing various oxygen concentrations in the stopped-flow spectrophotometer. All oxygen

concentrations used are at more than a 5-fold excess of the enzyme concentration to ensure pseudo-first order conditions.

Apparent rate constants (k_{obs}) were calculated from the kinetic traces using exponential fits and the software packages Kinetic Studio (Hi-Tech Scientific, Salisbury, UK) and Program A (written at the University of Michigan by Rong Chang, Jung-yen Chiu, Joel Dinverno, and David P. Ballou). Rate constants were obtained from oxygen using Marquardt-Levenberg nonlinear fit algorithms included in KaleidaGraph (Synergy Software). Simulations were performed by numerical methods using Runge-Kutta algorithms implemented in Berkeley Madonna 8.3 and a time-step of 2×10^{-4} s for simulations of the oxidative half-reaction of the enzyme-3HB complex. A five-step irreversible consecutive reaction model was used for simulations of the oxidative half-reaction.

Global analyses of absorption spectra acquired during oxidative half-reactions were performed using ReactLab^{TM} KINETICS (*Jplus consulting Ltd*), a software package used for calculation of intermediate spectra using multistep-irreversible consecutive reactions. The rate constants of each step were obtained from kinetic analysis of fits of single-wavelength kinetic traces.

To study solvent kinetic isotope effects (SKIE) on the oxidative half-reaction of 3HB6H, all enzyme solutions were exchanged into a Tris buffer made with deuterium oxide. In brief, Tris (hydroxymethyl) aminomethane (24.2 g) was dissolved in ~ 30 ml of 99.9% deuterium oxide, and the resultant solution was equilibrated for 13-15 hours (overnight) inside an anaerobic glove box (Belle Technology). The equilibrated solution was then evaporated at 60 $^{\circ}$C for 2 hours using a rotary evaporator to obtain H_2O-free Tris (hydroxymethyl) aminomethane powder. The resultant powder was dissolved in 99.9% deuterium oxide and the same process was repeated to ensure that the buffer contained at least 99.9% D_2O. The dried powder was then redissolved in ~195 ml of 99.9% D_2O. The buffer pD was adjusted by adding 1 M D_2SO_4 into the solution while monitoring the pD using a pH meter (pD = pH measured + 0.4) (21). The volume of the resulting buffer was adjusted to 200 ml with D_2O to obtain 100 mM Tris-D_2SO_4 pD 8.0. 3-Hydroxybenzoaic acid (3HB) (0.173 g) was dissolved in ~ 20 ml of 99.9% D_2O. The pD of the 3HB solution was adjusted to 8.0 by adding 0.1 M sodium deuterium oxide (NaOD). The solutions were dried twice as described above using a rotary evaporator. The dried powder of 3HB was re-dissolved in 25 ml of D_2O to obtain 50 mM 3HB in 100 mM Tris-D_2SO_4 pD 8.0. To avoid an exchange of deuterium with protium from air moisture, all processes were performed inside an anaerobic glove box. To prepare

enzyme in D_2O buffer, the concentrated enzyme solution (700 μL, A_{452} ~ 5.1) was equilibrated inside the anaerobic glove box for 30 minutes to remove oxygen. The solution was loaded onto a PD-10 column equilibrated with 100 mM Tris-D_2SO_4 pD 8.0 and the enzyme was eluted with D_2O buffer. The eluted enzyme solution was mixed with a solution of 3HB prepared in the same D_2O buffer and the volume was adjusted to ~6 ml to obtain a final absorbance at 452 nm of ~0.6 and a final concentration of 3HB ~10 mM. The enzyme-3HB complex in D_2O buffer was reduced by adding a solution of 0.5 mg/ml of dithionite solution, which was dissolved in D_2O buffer. Enzyme reduction was monitored using a spectrophotometer inside the anaerobic glove box to ensure stoichiometric reduction. The solution of reduced enzyme-3HB complex was transferred into a tonometer and left overnight (~ 18 hr) at 4 $^{\circ}C$ prior to the stopped-flow experiment. This preparation process was to assure that the enzyme was fully equilibrated in D_2O and that all of the exchangeable sites on the reduced enzyme had incorporated deuterium.

Analysis of the hydroxylation reaction using rapid-quench flow techniques. The experiments were performed using a TgK Scientific Model RQF-63, Dimention™ D1 rapid quench-flow system in an anaerobic glove box. The rapid quench-flow system consisted of three syringes. Syringe A contained an anaerobic solution of 25 μM reduced enzyme plus 10 mM 3HB. Syringe B contained a solution of quencher, 0.15 M HCl. Syringe C contained an air-saturated buffer (0.26 mM oxygen) plus 10 mM 3HB. The solution of reduced enzyme-3HB complex was mixed with the air-saturated buffer and the reaction mixture was allowed to age for various periods of time: 0.012 s, 0.015 s, 0.019 s, 0.024 s, 0.030 s, 0.037 s, 0.040 s, 0.046 s, 0.058 s, 0.062 s, 0.068 s, 0.090 s, 0.093 s, 0.134 s, 0.150 s, 0.230 s, 0.330 s, 0.430 s, or 0.530 s, before being quenched with 0.15 M HCl solution. Quenched samples were collected from the sample loop, and the enzyme was separated using a Microcon unit (Amicon YM-10). A solution of 1 M HCl was added to the filtrates to give a final concentration of 0.5 M HCl and the samples were analyzed for the amount of 2,5-DHB produced from the reaction using an HPLC (Agilent 1100 Series) with a 3.9 × 150 mm Nova-pak C18 reverse-phase column (Waters) and detected by a photodiode-array detector. The column was equilibrated with 5% methanol and 0.1% formic acid in H_2O as a mobile phase (flow rate of 0.5 ml/min) before sample injection. A gradient of methanol (increased from 5% to 40% in 20 min) and 0.1% formic acid was used to separate 3HB and 2,5-DHB. 2,5-DHB was identified by the absorbance at 330 nm and eluted at the retention time of 14.8 minutes after injection. The concentrations of product formed were estimated based on a standard curve in the range of 2-40

μM 2,5-DHB.

RESULTS

Reaction of free reduced enzyme with O_2 and the effects of NAD^+. A reduced enzyme solution was mixed with buffers containing various oxygen concentrations. Flavin oxidation was monitored at 10 nm intervals from 300 to 600 nm. No signs of formation of the intermediate C4a-hydroperoxyflavin were detected, as an increase of absorbance at all wavelengths was a single exponential (Figure 2A). A plot of the observed rate constants *versus* oxygen concentrations is linear without a significant intercept value, corresponding with a second-order rate constant of $4.96 \pm 0.4 \times 10^3$ $M^{-1}s^{-1}$ (inset in Figure 2A).

The effect of NAD^+ on the above reaction was investigated by mixing a solution of the reduced enzyme plus NAD^+ with oxygen-containing buffer using the double-mixing mode of the stopped-flow spectrophotometer. For the first mixing, the reduced enzyme (100 μM before mixing) was mixed with various concentrations of NAD^+ of 100 μM, 200 μM, 4 mM and 19.2 mM (concentrations before mixing) under anaerobic conditions. The resulting mixture was aged for 200 s to allow any binding of NAD^+ to take place before being mixed with buffer containing 1.92 mM oxygen (concentration before mixing) at the second mixing step. The final concentration of the enzyme was 25 μM, and those of NAD^+ were 25 μM, 50 μM, 1 mM and 4.8 mM. The reactions were monitored at 452 nm. The control reaction in which the reduced enzyme was mixed with anaerobic buffer without NAD^+ in the first mixing was also carried out. The results showed that the kinetic traces of the reaction of free enzyme without NAD^+, the reaction containing 25 μM NAD^+, and the reaction containing 50 μM NAD^+ were nearly the same, with observed rate constants of 1.98 ± 0.006 s^{-1}, 2.11 ± 0.03 s^{-1} and 2.20 ± 0.07 s^{-1}, respectively (as indicated by the arrow in Figure 2B). These data indicated that low concentrations of NAD^+ have no significant effect on the rate of enzyme oxidation. However, when NAD^+ concentrations were increased to 1 mM and 4.8 mM, the rate of enzyme oxidation was affected as the observed rate constants were 2.77 ± 0.07 s^{-1} and 5.23 ± 0.12 s^{-1}, respectively. These results imply that NAD^+ shows weak or non-specific binding to the reduced enzyme. However, as the reductive half-reaction only produces one equivalent of NAD^+, the data suggest that under turnover, NAD^+ hardly binds to reduced enzyme and likely leaves prior to the oxygen reaction.

Reaction of reduced enzyme-3HB complex with oxygen detected by stopped-flow spectrophotometry. A solution of the reduced enzyme plus 10 mM 3HB was mixed with buffers containing 10 mM 3HB and various oxygen concentrations in the stopped-flow spectrophotometer. Flavin oxidation was monitored at 10 nm intervals from 300 to 600 nm. In general, C4a-adduct intermediates (C4a-hydroperoxyflavin or C4a-hydroxyflavin) have their absorbance peaks around 360-410 nm with little absorption around 450 nm region. Therefore, formation and decay of C4a-hydroperoxyflavin and C4a-hydroxyflavin were detected at 400 nm while flavin oxidation was monitored at 452 nm (Figure 3A-B). At the initial time of measurement (0.002 s), the absorbance detected was different from absorbance of the reduced enzyme, indicating that part of the reaction of reduced enzyme-3HB complex and oxygen was rapid and occurred during the dead time of the stopped-flow mixing. The kinetics showed five exponential phases. At the highest oxygen concentration of 0.96 mM, where separation of each kinetic phase was the clearest, the first phase (0.002-0.003 s) was characterized by an increase in absorbance at 400 nm (Figure 3A) without an absorbance change at 452 nm. The plot of k_{obs} *versus* oxygen concentration was linear, yielding a second-order rate constant of 1.13 $\pm$ 0.01 × 10^6 $M^{-1}s^{-1}$ (inset in Figure 3B). The second phase (0.003-0.017 s) was characterized by a decrease in absorbance at 400 nm (Figure 3A). The observed rate constant of this phase was independent of oxygen concentration with an observed rate constant of 96 $\pm$ 3 s^{-1}. The kinetics of the decrease in absorbance at 400 nm of this phase was concurrent with an increase in absorbance at 452 nm (~16% change in the total amplitude) (Figure 3B). The third phase (0.017-0.060 s) showed an increase in absorbance at 400 nm independent of the oxygen concentration, and was consistent with an observed rate constant of 36 $\pm$ 2 s^{-1} (Figure 3A). This phase was also characterized by a major concomitant increase in absorbance at 452 nm (~82% change in the total amplitude).

The fourth phase (0.13-0.28 s) is a small amplitude change at 452 nm (~3% of total amplitude change at 452 nm), which can be fitted with a rate consent of 8-12 s^{-1} (Figure 3B). This phase is proposed to be a product release from the oxidized enzyme (this conclusion was later confirmed in page 11 of discussion). The trend of absorbance increase upon product leaving is also consistent with absorbance characteristics of the E_{ox}-product complex and free E_{ox} previously observed in (14). The fifth phase was a slow phase (~0.92 s^{-1}) with a small absorbance increase at 452 nm (~2 % of the total amplitude change) (Figure 3B). This phase might result from a small fraction of inactive enzyme because the rate constant of this step is much slower than the overall

turnover number of 6.49 ± 0.02 s^{-1} (Table 1). Therefore, the observed fourth phase was not included in the interpretation of the reaction mechanism. When the reduced enzyme-3HB complex was prepared using NADH as the reductant (stoichiometric reduction), and used in the same experiment as described above, the reduced enzyme-3HB complex in the presence of NAD^+ showed the same results (data not shown). These data again confirm that NAD^+ does not bind to the reduced enzyme-3HB complex.

Reaction of reduced enzyme-3HB complex with oxygen detected by rapid-quench techniques. Based on the stopped-flow data alone, the interpretation of each kinetic phase could not be assigned. Therefore, rapid-quench flow techniques (Experimental Procedures) were used to identify the hydroxylation rate constant. The results of the rapid-quench experiments gave a kinetic trace for product formation (filled-circle in inset of Figure 3A). For the stopped-flow experiment in which the oxygen concentration was the same as the rapid-quench experiment (0.13 mM after mixing), the observed rate constant of the first step (formation of C4*a*-hydroperoxyflavin) was 161 s^{-1} (k_{obs1}), that of the second step was 96 ± 3 s^{-1}, and that of the third step was 36 ± 2 s^{-1}. Therefore, simulations of product formation using a four-step irreversible consecutive reaction model with the hydroxylation rate constant of 96 s^{-1} (the second phase as the hydroxylation step, dotted line in inset of Figure 3A) or 36 s^{-1} (the third phase as the hydroxylation step, solid line in inset of Figure 3A) were carried out to identify the correlation between the rate constants measured from the stopped-flow and rapid-quench experiments. The comparison of rapid-quench data and simulations show that the simulation trace using the third step as the hydroxylation step (solid line) fits well with the experimental data while the other trace does not. Therefore, the third kinetic phase of the stopped-flow data reflects the step involved with product formation. As this phase is concurrent with flavin oxidation, it implies that the rate of C4a-hydroxyflavin decay is much faster than the rate of C4a-hydroxyflavin formation, thus preventing accumulation and detection of this intermediate. As a result, the overall kinetic mechanism of the oxidative half-reaction of 3HB6H can be summarized according to Figure 4.

According to the model in Figure 4, two forms of C4a-flavin adduct exist prior to the hydroxylation step. The first step is proposed to be formation of the C4a-peroxyflavin anion with an observed rate constant of 161 s^{-1} (k_1). The second step is bifurcation of the pathways of coupling (hydroxylation) and uncoupling (non-hydroxylation) paths. For the coupling path (82%), the proton transfer occurs to form the C4a-hydroperoxyflavin-3HB complex while for the uncoupling path

(16%), the H_2O_2 elimination takes place rapidly after the proton transfer to form the oxidized enzyme. The existence of the uncoupling pathway is also supported by results of product analysis and diode array detection (shown later). The observed rate constant of this phase (96 $\pm$ 3 s^{-1} (k_2)) is combined rate constants from both pathways and the spectrum *c* in Figure 6 is combined characteristics of C4a-hydroperoxyflavin-3HB complex and oxidized flavin. The third step is the hydroxylation step with a rate constant of 36 $\pm$ 2 s^{-1} (Table 1). The fourth step is the dehydration of C4a-hydroxyflavin to form oxidized flavin and H_2O. Because the hydroxylation step was observed at the same time as the majority of the flavin oxidation (~ 82% of the total amplitude change, Figure 3A-B), the data imply that the dehydration step (step 4, Figure 4) is rapid and could not be detected as a separate kinetic step.

Reaction of reduced enzyme-3HB complex with oxygen in the presence of sodium azide. It is known that the presence of inhibitory anions such as azide can slow down the dehydration step of C4a-hydroxyflavin in single-component flavoprotein hydroxylases (22-25). Therefore, we performed the experiment shown in Figure 3 in the presence of sodium azide (NaN_3) so that the identity of the C4a-hydroxyflavin could be resolved. At a concentration of 0.96 mM oxygen, the reaction containing 50 mM NaN_3 showed a kinetic trace with five exponential phases. For the kinetic traces detected at 400 nm (empty-circle line in Figure 5A), the first phase (0.002-0.003), the second phase (0.003-0.017 s), and the third phase (0.017-0.060 s) gave observed rate constants of 1500 s^{-1}, 96 s^{-1}, and 36 s^{-1} (the rate constant for hydroxylation), respectively, which are the same as for the reaction in the absence of sodium azide (Figure 3 , Table 1). For the traces detected at 452 nm, the data showed multiphasic kinetics similar to those observed at 400 nm. A notable effect of sodium azide addition was the presence of another intermediate which formed with the same rate constant as the hydroxylation step and decayed with a rate constant of 9.9 $\pm$ 0.2 s^{-1}.The decay step was concurrent with ~64% of the total absorbance increase at 452 nm. Therefore, this intermediate (empty-circle line in Figure 5B) was assigned as C4a-hydroxyflavin that dehydrates to form oxidized flavin. The fifth phase is a slow phase with a small absorbance increase at 452 (~ 2% of amplitude change) with a rate constant of 0.35 s^{-1}, which is probably due to a small inactive enzyme fraction similar to that observed in the reaction in the absence of azide. Altogether, the data clearly support the kinetic model proposed in Figure 4. The same experiments as in Figures 3 and 5 but with fluorescence detection were also carried out. However, the data were not useful for kinetic interpretation because only oxidized enzyme is fluorescent while none of the flavin

intermediates give fluorescence signals.

Product formation and hydroxylation ratio. The model in Figure 4 indicates that a fraction of C4a-hydroperoxyflavin bifurcates to form H_2O_2 without hydroxylating the substrate. Therefore, the percentage of 2,5-DHB formed per NADH consumed (coupling ratio) at pH 8.0 under the same conditions as the stopped-flow experiment was determined using an HPLC method (Experimental Procedures). The reaction was set with a limiting concentration of NADH (60 μM 3HB6H, 50 μM NADH, 10 mM 3HB) such that the reaction only occurs under single turnover. The results gave a coupling ratio of 86% which is consistent with the uncoupling ratio of ~16% observed in Figures 3-4. As the rate constant observed for decay of flavin hydroperoxide is the combined rate constant of the parallel reactions of H_2O_2 elimination. It is assumed that the fraction of ~ 86% of total enzyme carried out with hydroxylation whereas the fraction of ~ 14% was eliminated as hydrogen peroxide. Therefore, the rate constant for hydrogen peroxide elimination ($k^{H_2O_2}$) at the second step was ~ 13 s^{-1} (k_{10} in Figure 9). Simulations according to the model in Figure 4 agree well with the experimental data (dashed lines in Figure 3), validating the model in Figure 4 and the rate constants in Table 1.

Spectra of flavin intermediates involved in the reoxidation of 3HB6H. A similar experiment as those shown in Figures 3A-B in the presence of 3HB substrate was carried out, but with diode-array detection (Experimental Procedures). Global analysis of the data according to the model: $a \rightarrow b \rightarrow c \rightarrow d \rightarrow e \rightarrow f$, and with rate constants from the analysis of Figure 3A-B and from the simulations in Table 1 were used to identify the spectra of flavin intermediates involved in the reaction. Species *a* and *e* are the reduced enzyme-3HB complex and the oxidized flavin, respectively (Figure 6). The analysis yielded the filled-circle line which exhibits a maximum absorbance at 388 nm corresponding to the first intermediate (spectrum *b* in Figure 6). Spectrum *c* (empty-circle), which corresponds to the second intermediate, shows a peak absorbance at a shorter wavelength (378 nm) with an increase in absorbance in range of 440-500 nm of oxidized enzyme (~ 14%). According to the model in Figure 4, spectrum *b* represents the characteristic of C4a-peroxyflavin, while spectrum *c* represents the C4a-hydroperoxyflavin. Spectrum *d*, a third intermediate, shows characteristics of the oxidized enzyme that slowly converts to the final species, spectrum *e* (E'_{ox}) and *f* (E_{ox}) (as indicated by the arrow).

Solvent kinetic isotope effect (SKIE). Figure 4 proposes that the first two forms of oxygenated flavin adducts are C4a-peroxyflavin, resulting from the reaction of the reduced enzyme-3HB complex with

oxygen, and the C4a-hydroperoxyflavin that results from protonation of the first species. Therefore, the SKIE was used to verify whether the second step that is supposed to involve proton transfer was affected when the reaction was carried out in D_2O buffer (Experimental Procedures). The kinetic traces at 400 nm shown by the empty-circle line and by the solid line are those from experiments in D_2O and H_2O buffer, respectively (Figure 7A). When compared, both reactions showed that the first intermediate (which is supposed to be the C4a-peroxyflavin) formed maximally at 0.003 s and that no SKIE was detected for this step. The second phase (0.003-0.04 s) of the reaction in D_2O buffer (empty-circle line in Figure 7A) showed a lower rate constant of 56 $\pm$ 1 s^{-1} when compared to the reaction in H_2O buffer (96 s^{-1}), corresponding to a SKIE of 1.7. These results indicate that the second step involved proton transfer, supporting the reaction mechanism proposed in Figure 4. The third phase (0.04-0.2 s), which is supposed to reflect hydroxylation, also shows a lower rate constant of 19.9 $\pm$ 0.4 s^{-1} in D_2O buffer when compared to the data obtained for the H_2O experiment (36 $\pm$ 2 s^{-1}, Table 1), corresponding to a SKIE of 1.8. Although this phase is a combination of hydroxylation and dehydration, the SKIE value is contributed mainly by the hydroxylation step because the dehydration step is much faster than the hydroxylation. Altogether, the SKIE data support the reaction mechanism proposed in Figure 4.

Binding of 3HB to the reduced enzyme. The previous study has shown that 3HB binds to the oxidized enzyme via a single-step reaction with a k_{on} of 4 $\times 10^5$ $M^{-1}s^{-1}$ (k_1) and a k_{off} of 4600 s^{-1} (k_{-1}) (14). In this experiment, we investigated whether 3HB can also bind to the reduced enzyme if the enzyme was first reduced by NADH or dithionite. The experiment was performed using the double-mixing mode of the stopped-flow spectrophotometer. In the first mixing, a solution of the reduced enzyme was mixed with various concentrations of 3HB under anaerobic conditions and incubated for 50 s. This incubation period should be long enough to allow complete binding if a complex of the reduced enzyme and 3HB can form. In the second mixing, the solution from the first mixing was mixed with buffer containing 1.92 mM oxygen (before mixing concentration). The reaction was monitored at 400 nm to detect formation of C4a-hydroperoxyflavin (Figure 8A). The kinetic data in Figure 2 and Figure 3 could be used to distinguish the characteristics of the reaction in the absence or presence of substrate because in the absence of 3HB binding, the reaction would not form any C4a-hydroperoxyflavin (Figure 2A). Results in Figure 8A showed that the amplitude of the absorbance at 400 nm (characteristic of flavin C4a-adduct) increased with increased 3HB concentration, indicating that 3HB can bind to the reduced enzyme. The control

experiment in which the reduced enzyme was mixed with anaerobic buffer at the first mixing step did not result in any increase in absorbance at 400 nm at 0.004 s (dashed line in Figure 8A). Therefore, the increase in absorbance at 400 nm at 0.004 s was plotted against the concentration of 3HB in order to calculate the dissociation constant (K_d) of the reduced enzyme-3HB complex, giving a value of 0.077 $\pm$ 0.005 mM (inset in Figure 8A). For the third kinetic phase (0.017-0.060 s, Figure 8A) that corresponds to hydroxylation and flavin oxidation (Figure 4), the observed rate constants of this phase increased from 2.2 s^{-1} to 36 s^{-1} (lower to upper traces) when the substrate concentration was increased. This rate increment was due to the change in the rate of flavin oxidation as the enzyme was converted from the substrate-free to the substrate-bound form. The data also did not indicate any sign of substrate inhibition on the flavin oxidation step generally found in many *ortho*-hydroxylation flavoenzymes.

The kinetics for binding of 3HB to the reduced enzyme was also investigated using double-mixing mode. In the first mixing, the reduced enzyme was mixed with 20 mM 3HB (before mixing concentration) and incubated for various age times. The mixture from the first mix was added to an oxygenated buffer containing 10 mM 3HB in the second mix and the reaction was monitored for absorbance changes at 400 nm. An increase in absorbance at 400 nm due to the formation of C4a-hydroperoxyflavin was used as indication of the amount of reduced enzyme-3HB complex (Figure 8B), and this signal was plotted against the age time to yield the kinetics of complex formation. The analysis gave an observed rate constant of 7.3 $\pm$ 0.5 s^{-1} (inset in Figure 8B). A biomolecular rate constant of 3HB binding was calculated by dividing the observed rate constant with 10 mM 3HB as 7.3 $\pm$ 0.5 $\times$ 10^2 $M^{-1}s^{-1}$ (k_5 in Table 1, Figure 9). This calculation is valid because the dissociation rate constant (k_{off}) is small compared to the observed pseudo first-order rate constant. Based on the dissociation constant (K_d) of the reduced enzyme-3HB complex of 0.077 $\pm$ 0.005 mM (Figure 8A), the rate constant for dissociation of 3HB from the reduced enzyme-3HB complex (k_{off}) is equivalent to 0.056 s^{-1} (k_{-5} in Table 1, Figure 9).

DISCUSSION

This work reports on the kinetics of the oxidative half-reaction of 3HB6H from *R. jostii* RHA1 using various transient kinetic and mechanistic tools. The results reveal for the first time the catalytic features of a flavin-dependent *para*-hydroxylation reaction that are different as well as similar in many ways to the known reactions of *ortho*-hydroxylation. The data reported here are

also useful for understanding factors that control the overall catalysis. Although the overall structure of 3HB6H is similar to PHBH and other Class A flavoprotein monooxygenases, the arrangement of active site residues is rather different. In 3HB6H, the hydroxyl group of 3HB is proposed to make an H-bond interaction with a His213 residue, while the carboxylate group interacts with Gln49 and Tyr105 (17) (Figure 10). In PHBH, the hydroxyl group of pOHB makes an H-bond interaction with Tyr201 while the carboxylate group of the substrate interacts with Arg 214 (3) (Figure 10). The difference in active site structures presumably governs the opposite regio-specific hydroxylation between *ortho*- and *para*-hydroxylation enzymes and also contributes to the observed characteristics of 3HB6H that are different from PHBH, such as the presence of discrete steps in the formation of C4a-peroxyflavin and C4a-hydroperoxyflavin, and the absence of substrate inhibition on the flavin oxidation.

3HB6H is different from most of *ortho*-hydroxylation enzymes in that 3HB6H forms the C4a-peroxyflavin prior to protonation to form C4a-hydroperoxyflavin. This conclusion is drawn from the solvent kinetic isotope effect of 1.7 on the second step following the formation of the first intermediate, and from rapid-quench experiments which identified the hydroxylation step to be after formation of the second intermediate (Figure 3 and Figure 7). For other enzymes such as PHBH (26), MHPCO (24), and the oxygenase component of *p*-hydroxyphenylacetate hydroxylase (20, 27), the reaction with oxygen and proton transfer coincide because only the C4a-hydroperoxyflavin (not C4a-peroxyflavin) was detected as an intermediate prior to hydroxylation. An exception to this was found in the reaction of phenol hydroxylase (27) in which the enzyme showed formation of C4a-peroxyflavin anion before protonation to C4a-hydroperoxyflavin. The latter species is required in these aromatic hydroxylases because their reactions are involved in electrophilic aromatic substitution in which the C4a-hydroperoxyflavin acts as an electrophile (4, 7, 9). Although the advantage of having discrete steps of C4a-peroxyflavin and C4a-hydroperoxyflavin formation in 3HB6H and phenol hydroxylase is not clear, it highlights the differences in the proton transfer pathways among flavin-dependent hydroxylases.

In addition, 3HB6H does not exhibit substrate inhibition on the flavin oxidation step, a common characteristic found in *ortho*-hydroxylation enzymes. Substrate inhibition typically results in enzyme trapping in the form of C4a-hydroxyflavin, which prevents regeneration of the enzyme to the starting oxidized species. Many *ortho*-hydroxylation enzymes including PHBH (3, 5), phenol

hydroxylase (28), 2-methyl 3-hydroxypyridine 5- carboxylic acid oxygenase (24) and the oxygenase component of *p*-hydroxyphenylacetate hydroxylase (20, 27) are inhibited by excess substrate. The difference of 3HB6H from *ortho*-hydroxylation enzymes in this respect is probably attributable to the difference in substrate binding mode and the dynamics of ligand exchange. It remains to be seen in future investigation if the absence of substrate inhibition is also common in other *para*-hydroxylation enzymes.

The overall reaction of 3HB6H can be described according to a branched bimolecular mechanism model (29) in which an aromatic compound is the first substrate to bind to the enzyme to form the enzyme-substrate complex prior to NADH binding. The results in Figure 9 and from a previous study (14) indicate that another pathway in which NADH binds first and reduces the enzyme-bound FAD prior to aromatic substrate binding also exists (minor path in Figure 9). The data suggest that the path in which 3HB binds first is a preferred path because the binding occurs with a rate constant (k_{on}) of 4×10^5 $M^{-1}s^{-1}$ compared to a bimolecular rate constant of 43 $M^{-1}s^{-1}$ for the other path (14). For the reaction of PHBH, the binding of *p*-hydroxybenzoate and NADPH to the oxidized enzyme could be described as a random-order type (3, 23, 30). For other Class A flavoprotein monooxygenases, the sequence of substrate binding has not been fully explored as in the case of 3HB6H; however, it can be assumed that the flavin reduction by NAD(P)H is very slow unless a substrate is bound. This catalytic feature of Class A enzymes is advantageous for preventing NADH consumption and H_2O_2 production in the absence of aromatic substrate (physiological demand for hydroxylation reaction).

3HB6H shows a typical characteristic of Class A enzymes in that formation of C4a-adduct intermediates can only be detected in the presence of aromatic substrates (Figure 3A). The results in Figure 2B suggest that after the reduction of the enzyme-bound FAD by NADH is completed, NAD^+ is released prior to the oxygen reaction because there was no evidence showing any significant effect of NAD^+ on the oxidative half-reaction. The oxidation reaction of reduced-enzyme-3HB, prepared either by NADH or dithionite reduction, showed similar kinetics. For Class B flavoprotein monooxygenases such as phenylacetone monooxygenase (31), cyclohexanone monooxgenase (32), and L-ornithine monooxygenase (33-35), the binding of $NAD(P)^+$ is required to stabilize the C4a-peroxyflavin intermediate (36, 37). For Class C enzymes such as bacterial luciferase (38, 39) and Class D enzymes such as the oxygenase component of *p*-hydroxyphenylacetate hydroxylase (27, 40), C4a-hydroperoxyflavin can be detected in the absence

of any bound ligand.

Based on pre-steady state and steady state kinetics, the rate-limiting step for the overall reaction of 3HB6H is product release. Results from stopped-flow and rapid quench studies in previous and current reports unambiguously assign rate constants associated with individual steps. Under a similar condition to the pre-steady state kinetics studies, the apparent k_{cat} was measured as 6.49 $\pm$ 0.02 s^{-1} (Experimental Procedures, Table 1). Because there is no step with a rate constant in this range, the data suggest that product release (k_{12} in Figure 9) likely controls the overall rate of the reaction. Calculation of k_{cat} according to Equation 1 at saturation concentrations of all substrates according to the mechanism in Figure 9 can be described as in Equation 2 (derivations in Supporting Information):

$$k_{cat} = \left[\frac{1}{k_3k_4 + k_6(k_{-3} + k_4)} \times \left(\frac{(k_6(k_{-3} + k_4) + k_5(k_{-3} + k_3 + k_4))(k_8 + k_{10})}{k_5k_8}\right) + \frac{1}{k_{12}} + \frac{1}{k_{11}} + \frac{1}{k_9} + \frac{1}{k_8}\right]^{-1} \quad (2)$$

Using the individual rate constants and dissociation constants obtained from experimental data and simulations (Table 1), the value of k_{12} was calculated to be ~ 11.7 s^{-1}. This number also agrees well with the fourth phase of the stopped-flow data that is proposed to be the product release step (8-12 s^{-1}).

The kinetic mechanism of the reaction in Figure 9 indicates that both product release (k_{12} = 11.7 s^{-1}) and hydroxylation (k_9 = 36 s^{-1}) partially control the overall catalytic turnover. In order to confirm this conclusion, we measured the k_{cat} under the same condition in D_2O buffer (100 mM Tris-D_2SO_4 pD 8.0). The k_{cat} in D_2O was 5.43 $\pm$ 0.04 s^{-1} (Table 1), which corresponds to a SKIE of 1.2. These results support the conclusion above that the step predominantly controlling the overall reaction (k_{12} = 11.7 s^{-1}) is insensitive to D_2O, while the hydroxylation (k_9 = 36 s^{-1}), which has the intrinsic SKIE of 1.7 (Figure 7), partially controls the overall catalytic turnover. Therefore, the data in this report are useful in identifying that the hydroxylation and product release control the overall catalysis of 3HB6H. Although several flavoenzymes catalyzing *para*-hydroxylation of aromatic compounds have been reported (11), no detailed kinetic and mechanistic investigations of these enzymes have been carried out.

In conclusion, this study has elucidated the reaction mechanism of 3HB6H from *R. jostii* RHA1. The results clearly show that two forms of flavin C4a-adduct, C4a-peroxyflavin and C4a-hydroperoxyflavin, form prior to the hydroxylation step. The kinetic mechanism of 3HB6H can be described as a branched bimolecular mechanism in which 3HB is preferred to bind as the first substrate, followed by NADH that leaves prior to reaction with oxygen. The overall reaction of 3HB6H is controlled by hydroxylation and product release steps. These results represent the first report of the oxygenation mechanism of a *para*-hydroxylating flavoenzyme and serve as the grounds for future exploration of factors that govern the regio-specific hydroxylation at the *para*-position.

Acknowledgment

We thank Barrie Entsch for critical reading of the manuscript.

References

1. van Berkel, W.J., Kamerbeek, N.M., and Fraaije, M.W. (2006) Flavoprotein monooxygenases, a diverse class of oxidative biocatalysts. J. Biotechnol. 124, 670-689

2. Fagan, R.L., and Palfey, B.A. (2010) Comprehensive Natural Products II Chemistry and Biology: Flavin-dependent Enzymes, Elsevier: Oxford

3. Entsch, B., and Ballou, D.P. (2013) Handbook of Flavoproteins: The Reaction mechanisms of Groups A and B flavoprotein monooxygenases, Walter de Gruyter GmbH, Berlin/Briston

4. Ortiz-Maldonado, M., Ballou, D.P., and Massey, V. (1999) Use of free energy relationships to probe the individual steps of hydroxylation of p-hydroxybenzoate hydroxylase: studies with a series of 8-substituted flavins. Biochemistry 38, 8124-8137

5. Entsch, B., Cole, L.J., and Ballou, D.P. (2005) Protein dynamics and electrostatics in the function of p-hydroxybenzoate hydroxylase. Arch. Biochem. Biophys. 433, 297-311

6. Palfey, B.A., and McDonald, C.A. (2010) Control of catalysis in flavin-dependent monooxygenases. Arch. Biochem. Biophys. 493, 26-36

7. Chaiyen, P., Sucharitakul, J., Svasti, J., Entsch, B., Massey, V., and Ballou, D.P. (2004) Use of 8-substituted-FAD analogues to investigate the hydroxylation mechanism of the flavoprotein 2-methyl-3-hydroxypyridine-5-carboxylic acid oxygenase. Biochemistry 43, 3933-3943

8. Chaiyen, P. (2010) Flavoenzymes catalyzing oxidative aromatic ring-cleavage reactions. Arch. Biochem. Biophys. 493, 62-70

9. Tongsook, C., Sucharitakul, J., Thotsaporn, K., and Chaiyen, P. (2011) Interactions with the substrate phenolic group are essential for hydroxylation by the oxygenase component of p-hydroxyphenylacetate 3-hydroxylase. J. Biol. Chem. 286, 44491-44502

10. Montersino, S., and van Berkel, W.J. (2011) Functional annotation and characterization of 3-hydroxybenzoate 6-hydroxylase from Rhodococcus jostii RHA1. Biochim. Biophys. Acta 1824, 433-442

11. Montersino, S., Tischler, D., Gassner, G.T., and van Berkel, W.J. (2011) Catalytic and structural features of flavoprotein hydroxylases and epoxidases. Adv. Synth. Catal. 353, 2301-2319

12. Kallio, P., Patrikainen, P., Suomela, J.P., Mäntsälä, P., Metsä-Ketelä, M., and Niemi, J. (2011) Flavoprotein hydroxylase PgaE catalyzes two consecutive oxygen-dependent tailoring reactions in angucycline biosynthesis. Biochemistry 50, 5535-5543

13. Wang, Y., Niemi, J., and Mäntsälä, P. (2002) Modification of aklavinone and aclacinomycins in vitro and in vivo by rhodomycin biosynthesis gene products. FEMS Microbiol. Lett. 208, 117-122

14. Sucharitakul J, Wongnate T, Montersino S, van Berkel WJ, and Chaiyen, P. (2012) Reduction kinetics of 3-hydroxybenzoate 6-hydroxylase from Rhodococcus jostii RHA1. Biochemistry 51, 4309-4321

15. Joshi, R., Gangabhagirathi, R., Venu, S., Adhikari, S., and Mukherjee, T. (2012) Antioxidant activity and free radical scavenging reactions of gentisic acid: in-vitro and pulse radiolysis studies. Free Radic. Res. 46, 11-20

16. Ashidate, K., Kawamura, M., Mimura, D., Tohda, H., Miyazaki, S., Teramoto, T., Yamamoto, Y., and Hirata, Y. (2005) Gentisic acid, an aspirin metabolite, inhibits oxidation of low-density lipoprotein and the formation of cholesterol ester hydroperoxides in human plasma. Eur. J. Pharmacol. 513, 173-179

17. Montersino, S., Orru, R., Barendregt, A., Westphal, A.H., van Duijn, E., Mattevi, A., and van Berkel, W.H. (2013) Crystal structure of 3-hydroybenzoate 6-hydroxylase uncovers lipid-assisted flavoprotein strategy flavoprotein new strategy for regioselective aromatic hydroxylation. J. Biol. Chem. In Press.

18. Cha, S. (1968) A simple method for derivation of rate equations for enzyme-catalyzed reactions under the rapid equilibrium assumption or combined assumptions of equilibrium and steady state. J. Biol. Chem. 243, 820–825

19. Kuby, S.A. (2000) A Study of Enzymes: Chapter I, CRC Press: Florida.

20. Sucharitakul, J., Chaiyen, P., Entsch, B., and Ballou, D.P. (2006) Kinetic mechanisms of the oxygenase from a two-component enzyme, p-hydroxyphenylacetate 3-hydroxylase from Acinetobacter baumannii. J. Biol. Chem. 281, 17044–17053

21. Schowen, K.B., and Schowen, R.L. (1982) Solvent isotope effects of enzyme systems. Methods Enzymol. 87, 551-606

22. Steennis, P.J., Cordes, M.M., Hilkens, J.H., and Müller, F. (1973) On the interaction of p-hydroxybenzoate hydroxylase from Pseudomonas fluorescens with halogen ions. FEBS Lett. 36, 177-180

23. Entsch, B., Ballou, D.P., and Massey, V. (1976) Flavin-oxygen derivatives involved in hydroxylation by p-hydroxybenzoate hydroxylase. J. Biol. Chem. 251, 2550-2563

24. Chaiyen, P., Brissette, P., Ballou, D. P., and Massey, V. (1997) Unusual mechanism of oxygen atom transfer and product rearrangement in the catalytic reaction of 2-methyl-3-hydroxypyridine-5-carboxylic acid oxygenase. Biochemistry 36, 8060–8070

25. Chaiyen, P., Brissette, P., Ballou, D. P., and Massey, V. (1997) Reaction of 2-methyl-3-hydroxypyridine-5-carboxylic acid (MHPC) oxygenase with N-methyl-5-hydroxynicotinic acid: studies on the mode of binding, and protonation status of the substrate. Biochemistry 36, 13856–13864

26. Entsch, B., and van Berkel, W.J. (1995) Structure and mechanism of para-hydroxybenzoate hydroxylase. FASEB J. 9, 476-83

27. Ruangchan, N., Tongsook, C., Sucharitakul, J., and Chaiyen ,P. (2011) pH-dependent studies reveal an efficient hydroxylation mechanism of the oxygenase component of p-hydroxyphenylacetate 3-hydroxylase. J. Biol. Chem. 286, 223-233

28. Maeda-Yorita, K., and Massey, V. (1993) On the reaction mechanism of phenol hydroxylase. New information obtained by correlation of fluorescence and absorbance stopped flow studies. J. Biol. Chem. 268, 4134-4144

29. Keitaro, H. (1979) Kinetics of Fast Enzyme Reactions: Analysis of Fast Reactions: Transient Kinetics, Kodansha Ltd.: Tokyo

30. Husain, M., and Massey, V. (1979) Kinetic studies on the reaction of p-hydroxybenzoate hydroxylase. Agreement of steady state and rapid reaction data. J. Biol. Chem. 254, 6657-6666.

31.Torres Pazmiño, D.E., Winkler, M., Glieder, A., and Fraaije, M.W. (2010) Monooxygenases as biocatalysts: Classification, mechanistic aspects and biotechnological applications. J. Biotechnol. 146, 9-24

32.Sheng, D., Ballou, D.P., and Massey, V. (2001) Mechanistic studies of cyclohexanone monooxygenase: chemical properties of intermediates involved in catalysis. Biochemistry 40, 11156-11167

33. Chocklett ,S.W., and Sobrado, P. (2010) Aspergillus fumigatus SidA is a highly specific ornithine hydroxylase with bound flavin cofactor. Biochemistry 49, 6777-6783

34. Mayfield, J.A., Frederick, R.E., Streit, B.R., Wencewicz ,T.A., Ballou, D.P., and DuBois, J.L. (2010) Comprehensive spectroscopic, steady state, and transient kinetic studies of a representative siderophore-associated flavin monooxygenase. J. Biol. Chem. 285, 30375-30388

35. Meneely, K.M., Barr, E.W., Bollinger, J.M.Jr., and Lamb, A.L. (2009) Kinetic mechanism of ornithine hydroxylase (PvdA) from Pseudomonas aeruginosa: substrate triggering of O2 addition but not flavin reduction. Biochemistry 48, 4371-4376

36. Alfieri, A., Malito, E., Orru, R., Fraaije, M.W., and Mattevi, A. (2008) Revealing the moonlighting role of NADP in the structure of a flavin-containing monooxygenase. Proc Natl. Acad. Sci. USA. 105, 6572-6577

37. Orru, R., Dudek, H.M., Martinoli, C., Torres Pazmino, D.E., Royant, A., Weik, M., Fraaije, M.W., and Mattevi, A. (2011) Snapshots of enzymatic Baeyer-Villiger catalysis: oxygen activation and intermediate stabilization. J. Biol. Chem. 286, 29284-29291

38. Suadee, C., Nijvipakul, S., Svasti, J., Entsch, B., Ballou, D.P., and Chaiyen, P. (2007) Luciferase from Vibrio campbellii is more thermostable and binds reduced FMN better than its homologues. J. Biochem. 142, 539-552

39. Tinikul, R., Thotsaporn, K., Thaveekarn, W., Jitrapakdee, S., and Chaiyen, P. (2012) The fusion Vibrio campbellii luciferase as a eukaryotic gene reporter. J. Biotechnol. 162, 346-353

40.Thotsaporn, K., Chenprakhon, P., Sucharitakul, J., Mattevi, A., and Chaiyen, P. (2011) Stabilization of C4a-hydroperoxyflavin in a two-component flavin-dependent monooxygenase is achieved through interactions at flavin N5 and C4a atoms. J. Biol. Chem. 286, 28170-28180

41.Schreuder, H.A., Prick, P.A., Wierenga, R.K., Vriend, G., Wilson, K.S., Hol, W.G., and Drenth, J. (1989) Crystal structure of the p-hydroxybenzoate hydroxylase-substrate complex refined at 1.9 A resolution. Analysis of the enzyme-substrate and enzyme-product complexes. J. Mol. Biol. 208, 679-696

Table 1. Values of rate constants described in Figure 4 and 9.

The values were obtained from experimental data performed in 100 mM Tris-H_2SO_4 pH 8.0 at 4 °C using the stopped-flow spectrophotometer or kinetic simulations.

Observed rate constant from experimental data	Rate constants from simulations
$k_1 = 2.6 \pm 0.03 \times 10^5$ $M^{-1}s^{-1}$ [a]	$k_1 = 4 \times 10^5$ $M^{-1}s^{-1}$ [a]
$k_{-1} = 65 \pm 3$ s^{-1} [a]	$k_{-1} = 64 \pm 3$ s^{-1} [a]
—	$k_2 = 4.4 \times 10^6$ $M^{-1}s^{-1}$ [a]
—	$k_{-2} = 7600$ s^{-1} [a]
$k_3 = 377 \pm 8$ s^{-1} [a]	$k_3 = 340$ s^{-1} [a]
—	$k_{-3} = 12$ s^{-1} [a]
$k_4 = 48 \pm 2$ s^{-1} [a]	$k_4 = 51$ s^{-1} [a]
$k_5 = 7.3 \pm 0.5 \times 10^7$ $M^{-1}s^{-1}$ [b]	—
$k_{-5} = 0.056$ s^{-1}	—
$k_6 = 43 \pm 2$ $M^{-1}s^{-1}$ [a]	—
$k_7 = 1.13 \pm 0.01 \times 10^6$ $M^{-1}s^{-1}$	$k_7 = 1.6 \times 10^6$ $M^{-1}s^{-1}$ [d]
$k_8 + k_{10} = 96 \pm 3$ s^{-1}	
$k_8 = 83$ s^{-1} [e]	$k_8 = 83$ s^{-1} [d]
$k_9 = 36 \pm 2$ s^{-1}	$k_9 = 36$ [d]
$k_{10} = 13$ s^{-1} [e]	$k_{10} = 13$ s^{-1}
k_{11} (-NaN_3) = nd	—
k_{11} (+NaN_3) = 9.9 s^{-1}	—
$k_{12} = 11.7$ s^{-1} [c]	—
k_{13} (-NaN_3) = 0.92 s^{-1} [f]	—
k_{13} (+NaN_3) = 0.35 s^{-1} [f]	—
$k_{cat(app)}^{H_2O} = 6.49 \pm 0.02$ s^{-1}	

$k_{cat(app)}^{D_2O}$ = 5.43 ± 0.04 s^{-1}

[a]Rate constants from simulations and experimental data were according to the previous report (14).
[b]The apparent bimolecular rate constant
[c]The value was calculated from k_{cat} and Equation 2.
[d]The values from simulations according to Experimental Procedures and Figure 3.
[e]The values calculate from percent coupling (86%)
[f]The rate constant of fifth phase in Figure 3 which is not in catalytic cycle but only used for simulation with the experimental traces.

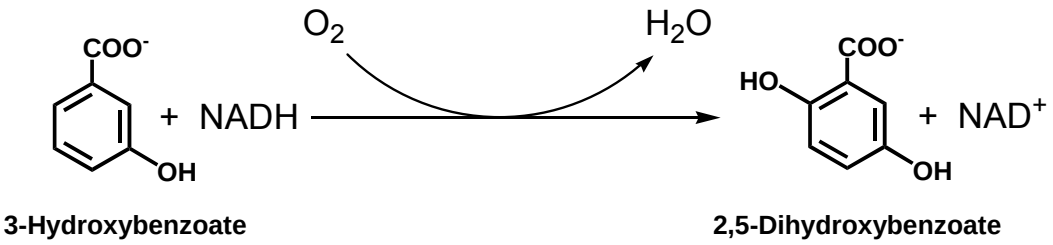

Figure 1. Catalytic reaction of 3HB6H.

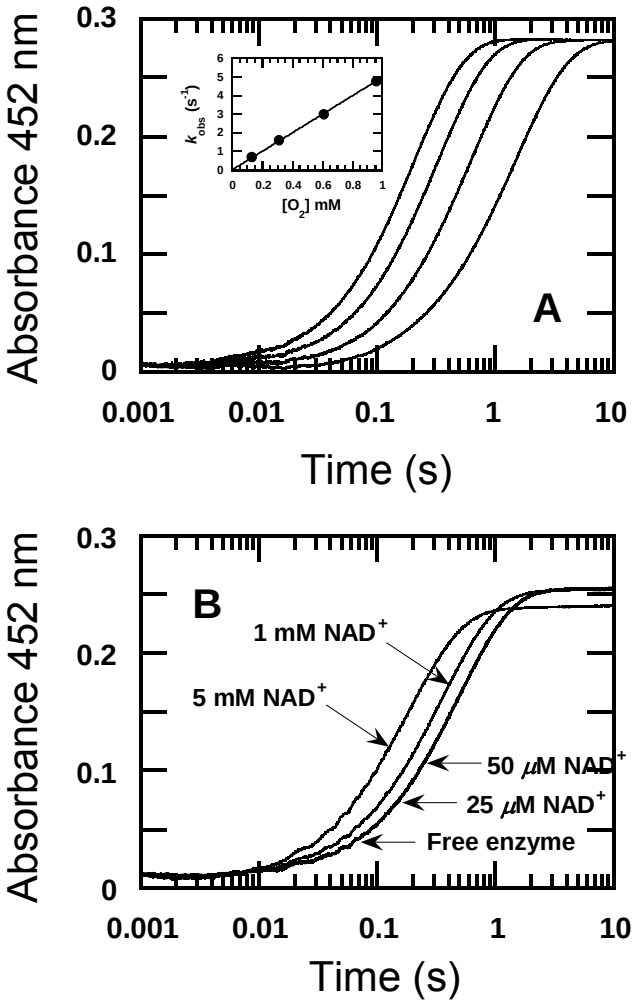

Figure 2. Reaction of free reduced 3HB6H enzyme with oxygen and the effect of NAD+ on the re-oxidation. (A) A solution of the reduced enzyme (26 μM) was mixed with buffer containing various oxygen concentrations, 0.13 mM, 0.31 mM, 0.61 mM and 0.96 mM in 100 mM Tris-H2SO4 pH 8.0 at 4 ºC. All given concentrations are after mixing. The reaction was monitored at a wavelength of 452 nm with a stopped-flow spectrophotometer. The kinetic traces from left to right correspond to increasing oxygen concentrations. Inset shows a plot of the observed rate constants versus oxygen concentrations. (B) A solution of the reduced enzyme (25 μM) was mixed with different NAD+ concentrations of 25 μM, 50 μM, 1 mM and 4.8 mM (indicated by arrows) under anaerobic

conditions in the first mixing. All concentrations are given as after mixing performed in 100 mM Tris-H2SO4 pH 8.0 at 4 ºC. The mixture solution of reduced enzyme and NAD+ was aged for 200 s and then the reaction was mixed with 0.61 mM oxygen in the second mixing. The oxidation reactions were monitored at 452 nm.

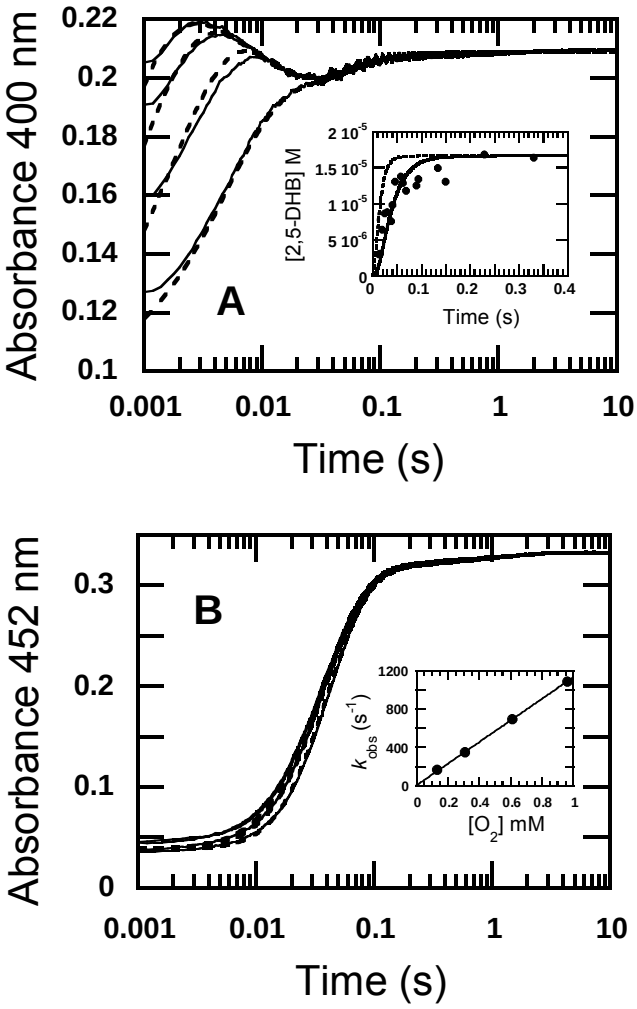

Figure 3. Reaction of reduced 3HB6H enzyme in the presence of 3HB with oxygen. A solution of the reduced enzyme (30 μM) plus 10 mM 3HB was mixed with buffer containing various oxygen concentrations of 0.13 mM, 0.31 mM, 0.61 mM and 0.96 mM, plus 10 mM 3HB in the stopped-flow spectrophotometer. All concentrations as described were after mixing. The reaction was performed in 100 mM Tris-H_2SO_4 pH 8.0 at 4 $^{\circ}$C. (A) The reaction was monitored by absorbance change at 400 nm to detect formation of C4a-flavin adduct intermediates and (B) at 452 nm for detecting flavin oxidation. The lower to upper kinetic traces at 400 nm correspond to increasing oxygen concentrations. The dotted lines are from simulations using a four-step consecutive reaction

according to $a \rightarrow b \rightarrow c \rightarrow d \rightarrow e \rightarrow f$. The rate constants of each step used for simulations are according to those indicated in Table 1, k_7 = 1.6 $\times 10^6$ $M^{-1}s^{-1}$, k_8 = 83 s^{-1}, k_9 = 36 s^{-1}, k_{10} = 13 s^{-1}, k_{12} = 11.7 s^{-1}, k_{13} = 0.92 s^{-1}, and the molar absorption coefficients used for the simulations were ε_{400} of *a* (E_{red}) = 3300 $M^{-1}cm^{-1}$, ε_{400} of *b* (*E*-C4a-peroxyflavin) = 7500 $M^{-1}cm^{-1}$, ε_{400} of *c* (*E*-C4a-hydroperoxyflavin) = 6300 $M^{-1}cm^{-1}$, ε_{400} of *d* (E_{ox}-2,5-DHB) = 6800 $M^{-1}cm^{-1}$, ε_{400} of *e* (E'_{ox}) = 6900 $M^{-1}cm^{-1}$, ε_{400} of (E_{ox}) = 6910 $M^{-1}cm^{-1}$ and at 452 nm, ε_{452} of *a* = 1200 $M^{-1}cm^{-1}$, ε_{452} of *b* = 1300 $M^{-1}cm^{-1}$, ε_{452} of *c* = 1400 $M^{-1}cm^{-1}$, ε_{452} of *d* = 10300 $M^{-1}cm^{-1}$, ε_{452} of *e* = 10600 $M^{-1}cm^{-1}$, ε_{452} of *f* = 11000 $M^{-1}cm^{-1}$. Inset 3A shows a plot of product formed *versus* time obtained from rapid quench-flow experiments (filled circles) under the same condition as those in the stopped-flow experiment. Simulations of product formation according to the model used in the main figures but with the observed hydroxylation rate constant of 36 s^{-1} at the second step or 96 s^{-1} at the third step are shown in solid and dotted lines, respectively. Inset 3B shows a plot of the observed rate constants *versus* oxygen concentrations.

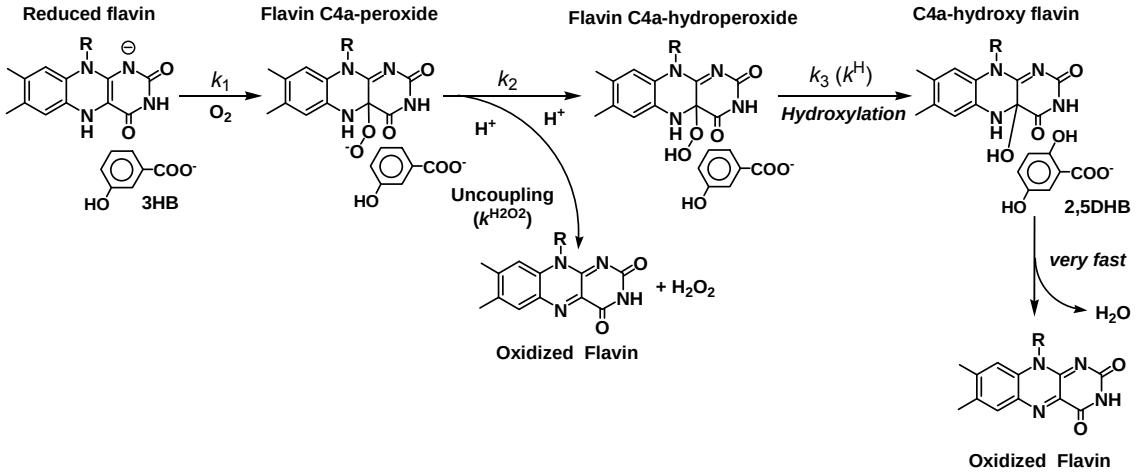

Figure 4. The oxygenation reaction of 3HB6H. The first step is formation of C4a-peroxy anion. The second step is a parallel reaction of protonation of a peroxy group to form C4a-hydroperoxyflavin and an uncoupling path for hydrogen peroxide elimination. The third step is a reaction of hydroxylation. The fourth step is dehydration of water from C4a-hydroxyflavin to return to the oxidized flavin, of which the reaction is very fast, preventing the detection of C4a-hydroxyflavin.

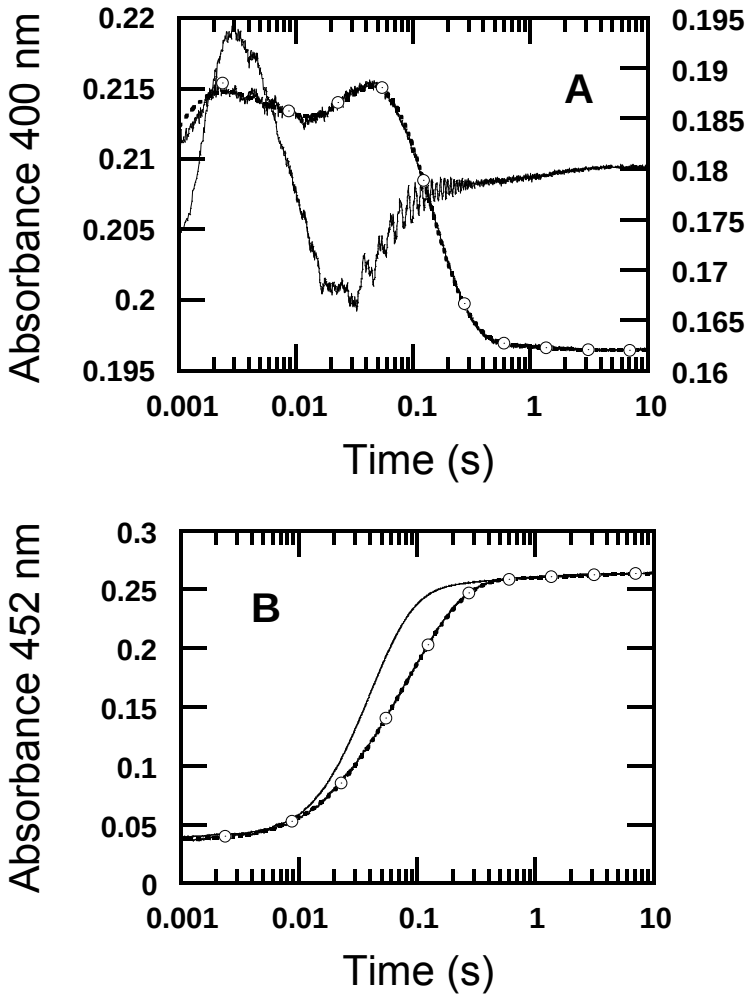

Figure 5. Reaction of reduced enzyme-3HB complex with oxygen in the presence of sodium azide. A solution of the reduced enzyme (23 μM) containing 10 mM 3HB and 50 mM sodium azide was mixed with buffer containing 10 mM 3HB, 50 mM sodium azide and 0.96 mM oxygen. All concentrations described were after mixing. The reactions were performed in 100 mM Tris-H_2SO_4 pH 8.0 at 4 $^{\circ}$C. (A) The reactions were monitored by absorbance change at 400 nm to monitor C4a-flavin adduct species. The empty-circle line was the kinetic trace in the presence of 50 mM sodium azide. Sodium azide slows down the rate of C4a-hydroxyflavin decay (from > 36 s^{-1} to

9.9 $\pm$ 0.2 s^{-1}) so that the existence of this intermediate can be identified (at 0.05 s) when compared to the same reaction without sodium azide (solid line trace). Simulations of the reaction in the presence of sodium azide are shown in dotted-line which is superimposed to the empty-circle line. The simulations used a five-step consecutive reaction according to a model, $a \rightarrow b \rightarrow c \rightarrow d \rightarrow e \rightarrow f$. Rate constants for each step used for simulations are according to those indicated in Table 1, k_7 = 1.6 $\times$ 10^6 $M^{-1}s^{-1}$, k_8 = 83 s^{-1}, k_9 = 36 s^{-1}, k_{10} = 13 s^{-1}, k_{11} (+NaN_3) = 10 s^{-1}, k_{13} = 0.35 s^{-1} and the molar absorption coefficients used for simulations were ε_{400} of *a* (E_{red}) = 4100 $M^{-1}cm^{-1}$, ε_{400} of *b* (*E*-C4a-peroxyflavin) = 8100 $M^{-1}cm^{-1}$, ε_{400} of *c* (*E*-C4a-hydroperoxyflavin) = 7500 $M^{-1}cm^{-1}$, ε_{400} of *d* (*E*-C4a-hydroxyflavin) = 8500 $M^{-1}cm^{-1}$, ε_{400} of *e* (E'_{ox}) = 6880 $M^{-1}cm^{-1}$, ε_{400} of *f* (E_{ox}) = 6887 $M^{-1}cm^{-1}$ and at 452 nm, ε_{452} of *a* = 1300 $M^{-1}cm^{-1}$, ε_{452} of *b* = 1700 $M^{-1}cm^{-1}$, ε_{452} of *c* = 2100 $M^{-1}cm^{-1}$, ε_{452} of *d* = 5900 $M^{-1}cm^{-1}$, ε_{452} of *e* = 10700 $M^{-1}cm^{-1}$, ε_{452} of *f* = 11000 $M^{-1}cm^{-1}$. (B) The reactions were monitored by absorbance change at 452 nm to detect flavin oxidation. The empty-circle line and the solid line were kinetic traces for the reaction with and without 50 mM sodium azide, respectively.

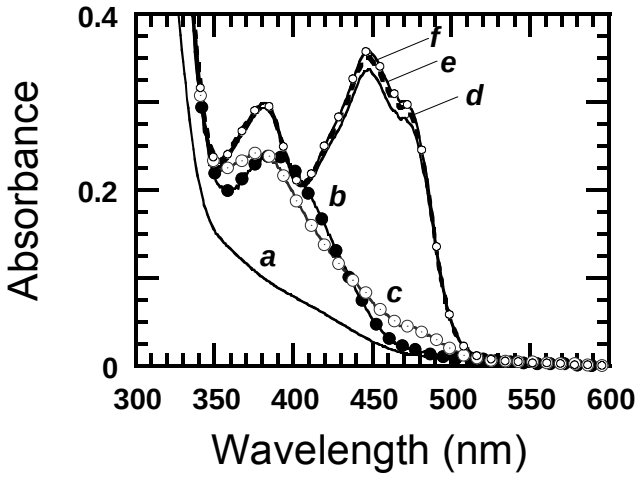

Figure 6. Spectra of intermediates in the reaction of reduced enzyme-3HB with oxygen. Reactions similar to those in Figure 3 were monitored using the stopped-flow diode-array spectrometer. All reactions were performed in 100 mM Tris-H_2SO_4 pH 8.0 at 4 $^{\circ}$C. (A) A solution of the reduced enzyme (32 μM) plus 10 mM 3HB was mixed with 0.96 mM oxygen plus 10 mM 3HB. All concentrations as described were after mixing. The solid line spectrum represents the reduced enzyme-3HB complex (*a*). Filled-circle and empty-circle lines are spectra of C4a-peroxyflavin anion (*b*) and of C4a-hydroperoxyflavin (*c*), respectively. Spectra *d* represents oxidized enzyme-2,5-DHB complex. Spectra *e* and *f* represent different forms of the free oxidized enzymes.

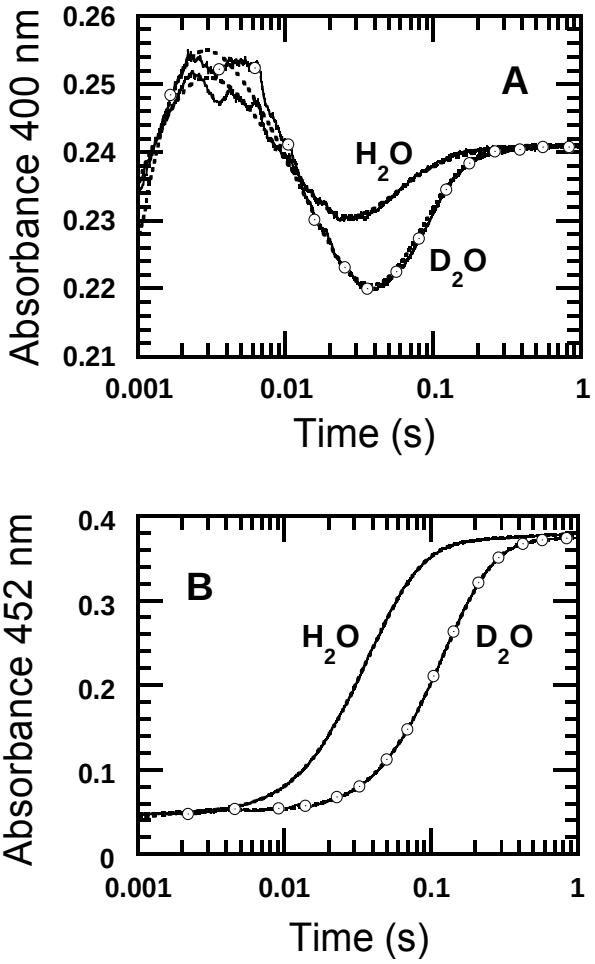

Figure 7. Reactions of reduced enzyme-3HB complex with oxygen in H_2O and D_2O buffers. A solution of the reduced enzyme (23 μM) containing 10 mM 3HB and 50 mM sodium azide was mixed with buffer containing 10 mM 3HB, 50 mM sodium azide and 0.96 mM oxygen. All concentrations described were after mixing. The reactions were performed in 100 mM Tris-H_2SO_4 pH (D) 8.0 at 4 $^{\circ}$C. (A) The reactions were monitored by absorbance change at 400 nm to detect formation of C4a-flavin adducts. Solid and empty-circle lines were the reactions in H_2O and D_2O buffer, respectively. (B) The reactions were monitored by absorbance change at 452 nm to detect

flavin oxidation. Solid and empty-circle lines were the reactions in H_2O and D_2O buffer, respectively. Dotted lines in A and B are kinetic traces obtained from simulations.

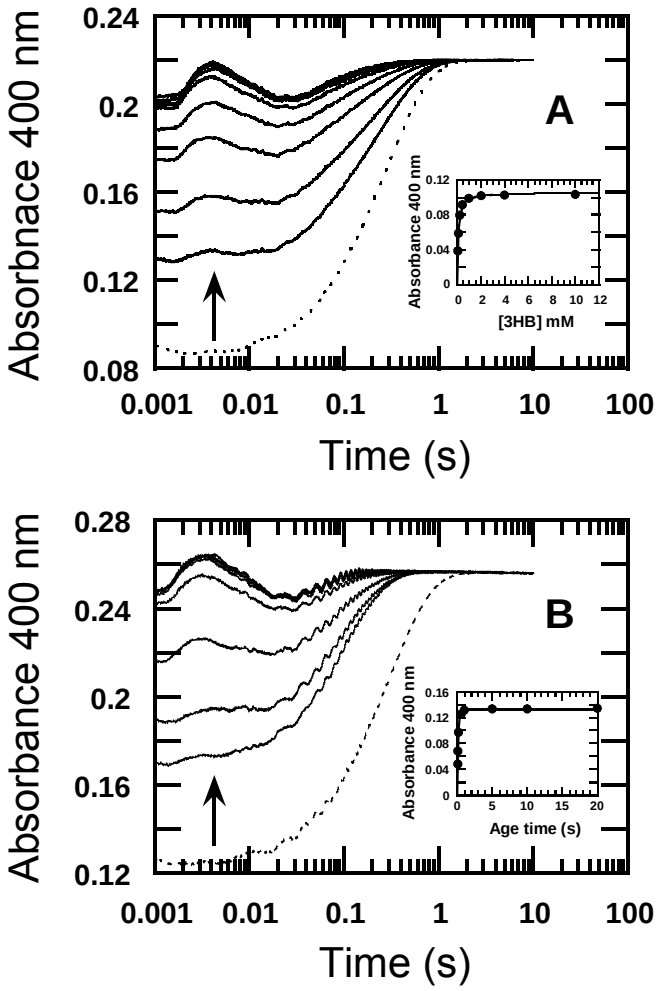

Figure 8. Binding of 3HB to the reduced enzyme. Experiments were performed using the double-mixing mode of the stopped-flow spectrophotometer. The reactions were performed in 100 mM Tris-H_2SO_4 pH 8.0 at 4 $^{\circ}$C. (A) In the first mixing, a solution of the reduced enzyme 127 μM (concentration before mixing) was mixed with buffer containing various 3HB concentrations, 0.1 mM, 0.2 mM, 0.4 mM, 0.8 mM, 2 mM, 8 mM and 20 mM (concentrations before mixing) under

anaerobic conditions. The mixture of reduced enzyme and 3HB was incubated for 50 s before it was mixed with buffers containing 0.96 mM oxygen and various 3HB concentrations of 0.05 mM, 0.1 mM, 0.2 mM, 0.4 mM, 1 mM, 4 mM and 10 mM. All concentrations were indicated according to before mixing conditions and the traces of low to high 3HB concentrations correspond to lower to upper traces (indicated by the arrow). The reactions were monitored at 400 nm to detect formation of C4a-hydroperoxyflavin. The increase of amplitude at 400 nm due to formation of C4a-hydroperoxyflavin represents the amount of the reduced enzyme-3HB complex. The dotted line trace is the control reaction without 3HB. Inset in A shows a plot of the absorbance change at 0.003 s *versus* the concentration of 3HB. (B) A solution of the reduced enzyme 120 μM (concentration before mixing) was mixed with 20 mM 3HB in the first mixing under anaerobic conditions. The reaction was incubated at various age times of 0.05 s, 0.1 s, 0.2 s, 0.5 s, 1 s, 5 s, 10 s and 20 s (indicated by arrow) before the mixture was mixed with buffer containing 1.92 mM oxygen and 10 mM 3HB (concentration as before mixing) in the second mix. The dotted line trace was a control reaction without 3HB. Inset in B shows a plot of the absorbance change at the time of 0.003 s *versus* age time.

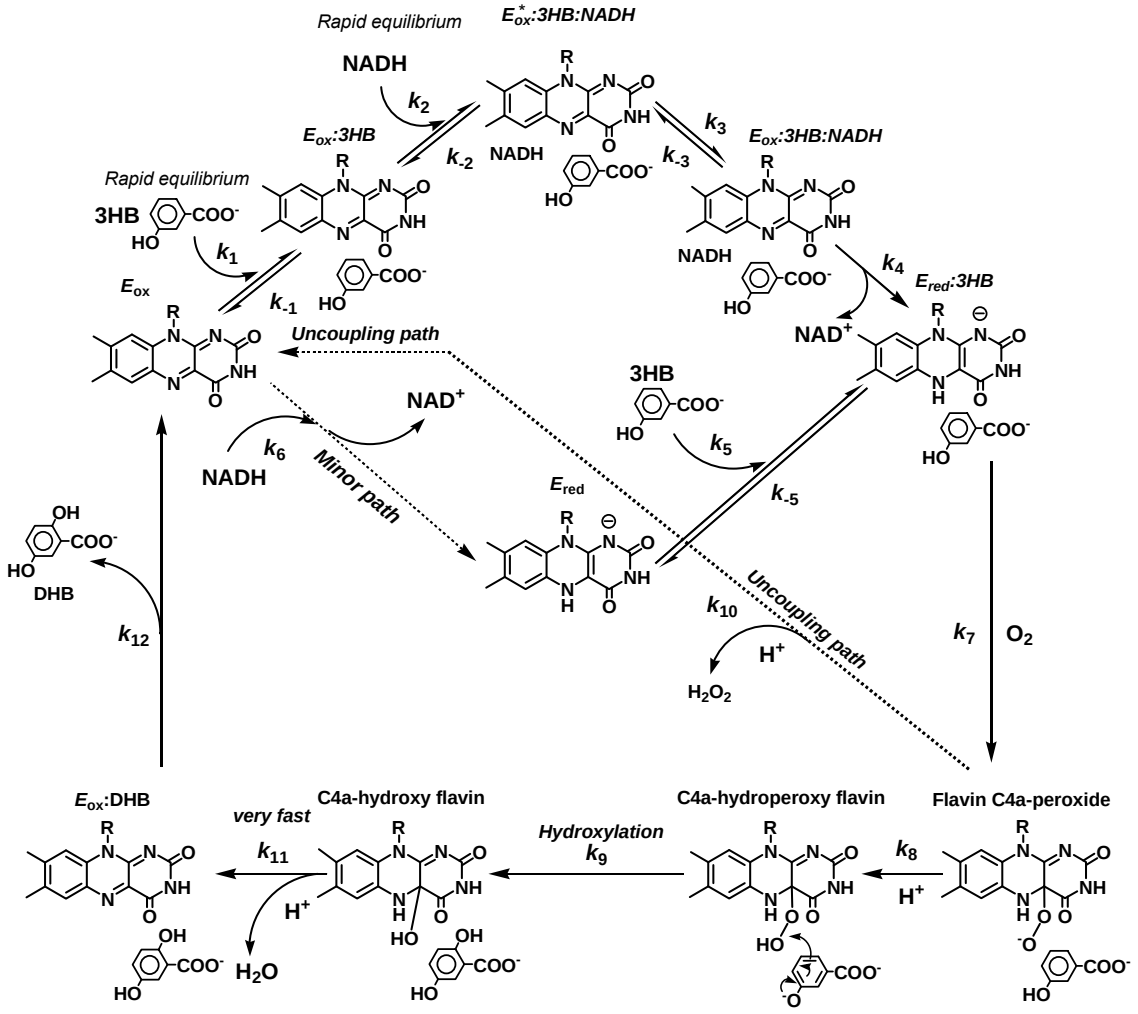

Figure 9. The kinetic mechanism for the overall reaction of 3HB6H. Reaction of 3HB and NADH to the oxidized enzyme can be described as a branched bimolecular mechanism. However, the binding of 3HB to the oxidized enzyme is more preferred (major path). This model was confirmed by kinetic simulations (shown in Figure 3).

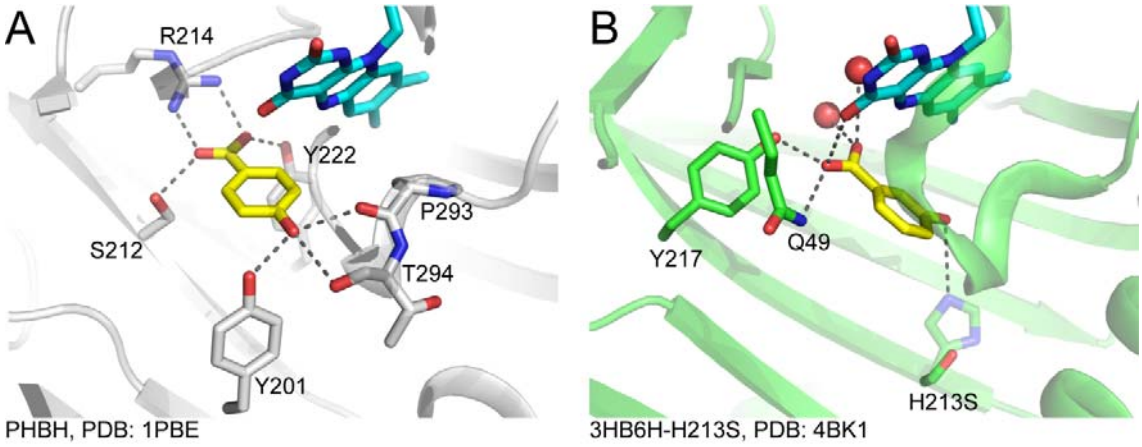

Figure 10. Comparison of active site structures of PHBH (*ortho*-hydroxylation) and 3HB6H (*para*-hydroxylation). (A) active site of PHBH (1PBE) (41), (B) active site of 3HB6H (4BK1) (17). The crystal structure of 3HB6H was obtained from co-crystallization of 3HB and the H213S variant of 3HB6H (17). A residue H213 in the wild-type enzyme was modeled by replacing S213 in the variant structure with His. The modeled H213 is shown in light color. The 3-OH group of 3HB may interact with H213.

Tyr217 and His213 are Important for Substrate Binding and Hydroxylation of 3-Hydroxy-benzoate 6-Hydroxylase from Rhodococcus jostii RHA1

Aromatic compounds and their derivatives are the largest groups of pollutants contaminating the environment [1]. Biodegradation of aromatic and phenolic compounds by microorganisms is an attractive approach for effective environmental remediation [2]. Microbes in the genus *Rhodococcus* have great potential in biodegradation applications [3] because they have a distinct cellular envelope composed of hydrophobic mycolic acid in addition to the phospholipids and fatty acids in their cellular membrane [4]. The composition of the cellular envelope promotes the entrance of hydrophobic molecules. These microbes can also produce biosurfactants that can help facilitate the transportation of toxic hydrophobic aromatics [5] and increase tolerance toward these compounds [4]. Phenols are important intermediates in the microbial degradation of aromatic compounds [6]. The catabolism of phenols generally requires the action of monooxygenases to generate diphenolic compounds such as catechol, procatechuate and gentisate that can be further degraded via an *ortho*-cleavage or *meta*-cleavage pathway by dioxygenases to result in intermediates that are part of central metabolic pathways [7].

3-Hydroxybenzoate 6-hydroxylase (3HB6H) from *Rhodococcus jostii* RHA1 is a flavoprotein monooxygenase that contains FAD as redox-active cofactor (8). The enzyme catalyzes the hydroxylation of 3-hydroxybenzoate (3HB) at the C6 position to form 2,5-dihydroxybenzoate (2,5-DHB) as a product (Fig. 1). 3HB6H is a member of group A flavoprotein monooxygenases [8,9]. 3HB6H differs from other well studied enzymes in this group in that it catalyzes regioselective *para*-hydroxylation instead of *ortho*-hydroxylation [8,10]. Furthermore, the enzyme is unique among flavoprotein monooxygenases in that it contains a tightly bound phospholipid ligand, which is involved in protein dimerization and in substrate binding [11]. The catalytic reaction of 3HB6H can be divided into reductive and oxidative half-reactions. The binding of aromatic substrate increases the rate of flavin reduction by NADH ~120 fold at a saturating concentration of NADH [12]. Investigations on the oxidative half-reaction have shown that C4a-peroxyflavin is the first species to be detected in the reaction of reduced enzyme and molecular oxygen. This intermediate is then protonated to form C4a-hydroperoxyflavin, a reactive intermediate that hydroxylates the substrate via an electrophilic aromatic substitution mechanism. Overall turnover is controlled by the

hydroxylation and product release steps [10]. Based on the crystal structure of the H213S variant with bound 3HB, the substrate binds on the *re* face of the flavin ring [11]. The residues Tyr217 and Gln49 interact with the carboxylate group of 3HB, while Ser213 points towards the 3-OH group of the substrate (Fig. 2). Presumably, for the wild-type enzyme, H213 interacts with the 3-OH group of 3HB [11]. The 3HB6H active site has several features that are different from other enzymes in the same class that catalyzes *ortho*-hydroxylation of aromatic compounds such as *p*-hydroxybenzoate 3-hydroxylase (PHBH), phenol hydroxylase and 2-methyl-3-hydroxypyridine-5-carboxlylic acid monooxgenase (MHPCO). In these *ortho* hydroxylases, interactions between ligand and enzymes are mediated through H-bonding networks of water. On the contrary, interaction between substrate and active site residues in 3HB6H is direct and not mediated through water or connected through outside solvent. As the previous study of phenol hydroxylase has shown that the residues located close to the OH-group of phenol is not involved in the hydroxylation, mechanistic investigation is required to establish the understanding of functional role of active site residues.

In this study, the functional roles of His213 and Tyr217 in the catalytic reaction of 3HB6H have been investigated using site directed mutagenesis and transient kinetics. The effects of mutation of these residues on substrate binding and hydroxylation were studied using stopped-flow and rapid-quench techniques. The results established Tyr217 as important for 3HB binding and His213 as crucial for substrate hydroxylation.

EXPERIMENTAL PROCEDURES

Reagents. NADH (purity $\geq$ 95%) and FAD (purity $\geq$ 95%) were purchased from Sigma-Aldrich. 3-Hydroxybenzoic acid (3HB) and 2,5-dihydroxybenzoic acid (2,5-DHB) were purchased from Merck. Concentrations of the following compounds were determined using the known absorption coefficients at pH 8.0: NADH, ε_{340} = 6.22 $\times$ 10^3 $M^{-1}cm^{-1}$; FAD, ε_{450} = 11.3 $\times$ 10^3 $M^{-1}cm^{-1}$; 3HB, ε_{288} = 2.0 $\times$ 10^3 $M^{-1}cm^{-1}$; 2,5-DHB, ε_{320} = 4.1 $\times$ 10^3 $M^{-1}cm^{-1}$. All of the absorption coefficient values are for the compounds in solution at pH 8.0.

Based on the crystal structure of 3HB6H:3HB complex, His213 and Tyr217 were selected as targets for site-directed mutagenesis [11]. The plasmid (pBAD) containing the 3HB6H gene [8] which has a His_6-tag at the N-terminus was amplified to remove the His_6-tag. The restriction sites for *Nde*I and *BamH*I were incorporated into the forward and reverse primers, respectively. The 3HB6H gene containing both restriction sites was amplified by PCR and then subcloned into the

pET-11a vector. The vector containing the wild-type enzyme was used as the template for carrying out site directed mutagenesis at the His213 and Tyr217 positions. The enzyme variants were purified according to the protocol used for the WT enzyme as previously described [12].

Molar absorption coefficients of the enzyme-bound FAD of 3HB6H variants were determined by adding 0.2% SDS as previous described [12]. The concentration of released free FAD was calculated on the basis of a molar absorption coefficient for free FAD (ε_{450}) of 11.3 mM^{-1} cm^{-1}. The molar absorption coefficients (one FAD per subunit) were calculated based on the absorption spectra of individual variants in relative to released free FAD concentration. These values are presented in Table 1.

All variants were stable in 100 mM sodium phosphate and 100 mM sodium sulfate pH 8.0, and the enzymes were kept for long-term storage in this buffer at -80 °C.

Spectroscopic Studies. UV-visible absorption spectra were recorded using a Hewlett-Packard diode array spectrophotometer (HP8453), a Shimadzu 2501PC spectrophotometer or a Cary 300Bio double-beam spectrophotometer at 25 °C. All spectrophotometers were equipped with thermostated cell compartments. Typical assays contained 10 mM 3HB, 2 μM FAD and 1 mM NADH. The enzyme activity was measured by monitoring the decrease in absorbance at 395 nm (decrease of NADH with ε_{395} = 0.22 × 10^3 $M^{-1}cm^{-1}$) over a time range that still gives good linearity for enzyme assays.

Dissociation Constants of Enzyme−Ligand Complexes. Binding experiments were conducted in 100 mM sodium phosphate and 100 mM sodium sulfate (pH 8.0) at 25 °C. Perturbation of flavin association with the 3HB6H variants upon substrate binding was measured using a split-beam spectrophotometer to record difference spectra. Two cuvettes, each containing a solution of ~25 μM enzyme were placed in the sample and reference cells. Equal volumes of the substrate and the buffer solution were added to the sample and reference cuvette, respectively. Wavelengths giving the highest amplitude change for each variant enzyme were selected for analysis. The dissociation constant (K_d) values for enzyme-ligand binding were obtained from plots of absorbance changes *versus* total substrate concentrations. The K_d was determined according to equation 1 using the Marquardt−Levenberg nonlinear fitting algorithms included in the KaleidaGraph Analysis Software (Synergy Software) where E_T is the total enzyme concentration, L_T is the total substrate concentration, ΔA and ΔA_{max} are the absorbance changes obtained at a given substrate

concentration and at a substrate saturated concentration, respectively. The K_d values of variant enzyme:3HB complexes obtained from static titration experiments are presented in Table 1.

$$\Delta A = \Delta A_{max} \frac{(E_T+L_T+K_d)-\sqrt{(E_T+L_T+K_d)^2-4E_TL_T}}{2E_T} \quad (1)$$

For the Tyr217 variants (Y217A, Y217S, Y217F) in which spectral perturbation from 3HB binding was not significant (Fig. S1, Supporting Information), the ultrafiltration method using a centriprep concentrator (YM10, 6 ml) with a 10 kDa molecular weight cut off was used to determine free 3HB concentrations upon incubation of the enzyme with varying 3HB concentrations of 0.2 mM, 0.4 mM, 0.9 mM, 1 mM, 2.5 mM, 3.6 mM, 5.8 mM, 7.9 mM, 12 mM and 15.7 mM. The enzyme concentration used was 10 μM. A solution of 3HB was added into the enzyme solution in a total volume of 6 ml. The mixture was centrifuged at 3000 rpm, 4 $^{\circ}$C for 2 min to obtain a volume of filtrate of less than 800 μl. The filtrate was diluted for the absorbance reading and the free 3HB concentration was determined based on the known extinction coefficient of 3HB at 288 nm (Experimental Procedures).

Rapid Reaction Experiments. Reactions were carried out in 100 mM sodium phosphate and sodium sulfate (pH 8.0) at 4 ºC, unless otherwise specified. The measurements were performed using a TgK Scientific Model SF-61DX or a TgK Scientific Model SHU-61SX2 stopped-flow spectrophotometer in single-mixing mode. The stopped-flow apparatus was made anaerobic by flushing the flow system with an anaerobic buffer solution containing 0.5 mg/ml dithionite in 100 mM sodium phosphate pH 8.0, and a dithionite solution was left in the flow cells overnight. The flow system of the stopped-flow instrument was washed with anaerobic 100 mM sodium phosphate and sodium sulfate (pH 8.0) three times before starting the experiments.

For preparation of a reduced enzyme solution, an anaerobic oxidized enzyme solution was placed in a tonometer and reduced with an equivalent amount of dithionite (0.2 mg/ml in 100 mM sodium phosphate and sodium sulfate pH 8.0), which was delivered from a gas-tight syringe with a microtitrator attached to the tonometer. The enzyme reduction was monitored through a cuvette attached to the tonometer to ensure a stoichiometric reduction process. The reduced enzyme solution was mixed with buffers containing various oxygen concentrations in the stopped-flow spectrophotometer. All oxygen concentrations used were in > 5-fold excess of the enzyme concentration to ensure pseudo-first order conditions.

Observed rate constants (k_{obs}) were obtained from the kinetic traces using exponential fits and the software packages Kinetic Studio (Hi-Tech Scientific, Salisbury, UK) and Program A (written at the University of Michigan by Rong Chang, Jung-yen Chiu, Joel Dinverno, and David P. Ballou). Bimolecular rate constants from the reactions of reduced enzyme with oxygen were obtained using Marquardt-Levenberg nonlinear fit algorithms included in KaleidaGraph (Synergy Software). Simulations were performed by numerical methods using Runge-Kutta algorithms implemented with Berkeley Madonna 8.3 software, using a time-step of 2×10^{-4} s for simulations of the oxidative half-reaction of the enzyme-3HB complex. Kinetic simulations are useful to suggest possible reaction models that are consistent with observed data. The percentage of product obtained from simulation was compared to the amount of product measured from single-turnover experiments to further rule out non-relevant models and point toward the simplest and valid model based on current evidence. A model providing simulation traces that are consistent with the experimental data was chosen as the model for explaining the kinetic mechanism of the variant.

Determination of Apparent Catalytic Constants ($k_{cat(app)}$). The $k_{cat(app)}$ values of 3HB6H variants were determined using enzyme monitored turnover. The experiments were performed under the same conditions as the rapid kinetic experiments. The oxidized enzymes (with absorbance of oxidized flavin of 0.3 after mixing) in the presence of 10 mM 3HB in air saturated buffer (~0.26 mM O_2) were mixed with buffer containing 1.03 mM O_2, 10 mM 3HB plus 20 mM NADH. The reaction was followed by monitoring the change in absorbance of the flavin cofactor over time which corresponds to the amount of oxidized enzyme under oxygen-limiting conditions (0.645 mM O_2). The reaction was followed until the oxygen was depleted. The steady-state period was defined as the period in which no change in absorbance of the oxidized enzyme was detected. The first derivative analysis of the kinetic trace was used to determine the precise time in which steady state is reached (t_{ss}). The $k_{cat(app)}$ was calculated using 0.645 mM $O_2/(t_{ss} \times E_t)$ where E_t is the total enzyme concentration (~28 μM) based on calculation using the molar absorption coefficients (cf. Table 1).

Analysis of the Hydroxylation Reaction Using Rapid-quench Flow Techniques. The experiments were performed using a TgK Scientific Model RQF-63 and Dimention™ D1 rapid quench-flow system in an anaerobic glove box. The rapid quench-flow system consisted of three syringes. Syringe A contained an anaerobic solution of ~25 μM reduced enzyme plus 10 mM 3HB in 100 mM sodium phosphate and 100 mM sodium sulfate pH 8.0. Syringe B contained a quench solution

of 0.6 M HCl. Syringe C contained an air-saturated buffer (~0.26 mM oxygen) plus 10 mM 3HB in 100 mM sodium phosphate and 100 mM sodium sulfate pH 8.0. The solution of reduced enzyme-3HB complex was mixed with the air-saturated buffer and the reaction mixture was allowed to age for various periods of time before being quenched with 0.6 M HCl. Quenched samples were collected from the sample loop, and the enzyme was separated using a Microcon concentrator (Amicon YM-10). The samples were analyzed for the amount of 2,5-DHB produced from the reaction using an HPLC (Agilent 1100 Series) with a 3.9 × 150 mm Nova-Pak C18 reverse-phase column (Waters) and detected by a photodiode-array detector. The column was equilibrated with 0.1% formic acid in H_2O (flow rate of 0.5 ml/min) before sample injection. A gradient of methanol was applied from 0% to 31% in 0.1% formic acid over 2 min and then maintained at 31% methanol in 0.1% formic acid to separate 2,5-DHB, 3HB and 2,3-DHB over 15 min. The pure compounds of 2,5-DHB, 3HB and 2,3-DHB were eluted at the retention times of 9.0 min, 10.4 min, 10.9 min after injection, respectively. These compounds were detected by their absorbance at 320 nm. The concentrations of product formed were estimated based on a standard curve over a range of 2-180 μM 2,5-DHB.

Analysis of the Product Formation from Single-turnover Reaction. Solutions of oxidized enzyme (~25 μM) plus 10 mM 3HB in 100 mM sodium phosphate and 100 mM sodium sulfate pH 8.0 were equilibrated inside the anaerobic glove box for 30 min. The enzyme solution (1.0 ml) was reduced with a dithionite solution (0.2 mg/ml) which was freshly prepared by dissolving the powder with the same anaerobic buffer. The solution of reduced enzyme-3HB complex in a well-sealed falcon tube was transferred outside the anaerobic glove box. The solutions were incubated in a water bath at 4 $^{\circ}$C for 10 min, and then mixed with an equal volume of air saturated solution of 10 mM 3HB in 100 mM sodium phosphate and 100 mM sodium sulfate pH 8.0 at the same temperature. The reaction mixtures were incubated for 5 min to ensure completion and then quenched with 0.3 M HCl (final concentration of 0.3 M). The enzyme and substrate/product were separated using a stir cell Microcon (Amicon YM-10) before HPLC analysis.

RESULTS

Thermodynamics and Kinetics of 3HB Binding to 3HB6H. Upon titration with 3HB, the flavin absorbance spectra of the H213 variants mostly showed a decrease in absorbance around 360-410 nm and 450-520 nm (Fig 3). In contrast, the Tyr217 variants including Y217A, Y217F and

Y217S did not show any significant spectral perturbation upon 3HB binding to the oxidized enzymes (Fig S1, Supporting Information). The binding of 3HB to these enzyme variants was further investigated using ultrafiltration. The results did not show evidence supporting 3HB binding to these enzymes because the 3HB concentration in the filtrate linearly correlated with the total 3HB concentration added (Fig. S2, Supporting Information), indicating that the K_d values for complex formation between 3HB and these variants are very high. The Tyr217A, Tyr217F and Tyr217S variants formed low amounts of 2,5-DHB product (4.6 $\pm$ 1 % 3.3 $\pm$ 2% and 3.7 $\pm$ 3, % respectively) (Table 2) and C4a-hydroperoxyflavin could not be detected during the transient kinetics experiments (Figure S3, Supporting Information). These data suggested that mutation of Tyr217 severely perturbs the ligand binding ability of the enzyme, and thus Tyr217 is important for 3HB binding.

To investigate the kinetics of 3HB binding of His213 variants, solutions of oxidized enzymes (~30 μM after mixing) were mixed with 3HB using the stopped-flow spectrophotometer. The binding reactions for H213A, H213S, H213E and H213D were followed by monitoring the decrease in absorbance at 487, 488, 480 and 490 nm, respectively (Fig. 4). These wavelengths gave maximal spectral perturbation based on static titration experiments (Fig. 3). Among these variants, the binding of 3HB to H213S was the fastest (k_{obs} >> 1000 s^{-1}) because all amplitude changes occurred during the dead time of stopped-flow mixing (solid lines in Fig. 4), while the binding to H213A, H213E and H213D to the substrate is slower because part of the absorbance change could be detected after the stopped-flow dead time. Simulations were used for analyzing the kinetics of 3HB binding to these variants because large parts of the data were lost during the dead time. The binding of 3HB to all His213 variants (except H213S) was interpreted as a single-step binding process, which is similar to the wild-type enzyme [12]. The dotted lines represent the simulations according to a single-step binding model, which agrees well with the experimental data (solid lines in Fig. 4). All His213 variants showed bimolecular rate constants (k_f^{sim}) and reverse rate constant (k_r^{sim}) in the same range as those of the wild-type enzyme (Table 1). For H213S, the binding reaction finished during the dead time of the stopped-flow mixing, and the data could only be used to estimate a K_d value at 4 °C of 0.42 $\pm$ 0.012 mM. All results indicated that the ligand binding properties of the His213 variants are similar to the wild-type enzyme (Table 1).

Product Formation of Enzyme Variants under Single-Turnover Reactions and Rapid Quench Experiments. A solution of reduced enzyme plus 10 mM 3HB was mixed with air-saturated buffer

containing 10 mM 3HB. The experiment was used to investigate the effect of mutation on both the substrate hydroxylation and the regioselectivity of the hydroxylation. The results showed that H213A could not form any product, whereas H213E showed a higher efficiency (92%) of hydroxylation than the wild-type enzyme (86%) (Table 2). Other His213 variants showed partial uncoupling of hydroxylation (Table 2). Product analysis also indicated that all active variants (including the Tyr217 variants) exclusively catalyze *para*-hydroxylation.

Rapid quench experiments were also used to measure the observed rate constants of hydroxylation as shown in Table 2. The data indicated that the substitution of His213 with Ala, Ser and Asp lowers the rate of substrate hydroxylation as well as the efficiency of product formation. Interestingly, H213E behaves similarly to the wild-type enzyme and is slightly more efficient in product formation.

Identification of the Ionic State of 3HB Bound to 3HB6H. Only H213E was chosen for this experiment because its K_d value is less than that of the wild-type enzyme and the hydroxylation was not affected by mutation (Table 1). The three-buffer system was used to maintain the same ionic strength throughout the pH range investigated [13]. Free 3HB spectra under different pH conditions were first recorded. The spectrum of fully protonated 3HB (at the carboxylic and phenolic moieties) showed a single peak at 296 nm (at pH 0.54, Fig. S4, Supporting Information). The spectrum of mono-anionic 3HB (the carboxylate and phenolic form) showed a single peak at 288 nm (at pH 8.0, Fig. S4, Supporting Information). The spectrum of di-anionic 3HB in the carboxylate/phenolate form showed a single peak at 312 nm (at pH 12.0, Fig. S4, Supporting Information). Based on the K_d for 3HB binding to H213E (K_d = 52 μM, Table 1), a solution of 15 μM H213E and 20 μM 3HB should result in 3.6 μM of the H213E:3HB complex. The observed spectrum representing both 16.4 μM free 3HB and 3.6 μM of enzyme-bound 3HB as shown in Fig. 5 by the dotted line B is similar to the spectrum of the phenolic form of 3HB recorded at pH 8.0 (solid line A, Fig. 5). This also indicated that the spectrum of enzyme-bound 3HB is not significantly different from free 3HB. The spectrum of 16.4 μM free 3HB was subtracted from spectrum B, to give the spectrum of 3.6 μM enzyme-bound 3HB, as shown by the dotted line C. The spectrum showed two peaks at 270 nm and at 288 nm (Fig. 5). The peak at 288 nm is similar to the peak typically characteristic of the phenolic form of free 3HB in buffer pH 8.0 shown in spectrum A (Fig. 5). If 3HB (3.6 μM) is deprotonated to form the phenolate form, the peak should have shifted to 312 nm as shown in spectrum D (solid line in Fig. 5). The perturbation of

absorption around 440-510 nm or 350-420 nm also confirms that under these conditions, 3HB still binds to the enzyme active site (Fig. 3). All of the results suggested that at pH 8.0, 3HB likely binds to the oxidized enzyme in the phenolic form.

Kinetics of the Reaction of the Reduced H213A:3HB Complex with Oxygen. To gain further insight into the functional role of His213 in substrate hydroxylation, the pre-steady state kinetics of the His213 variants were investigated. Solutions of the reduced enzyme variants plus 10 mM 3HB were mixed with buffer containing 10 mM 3HB and various concentrations of oxygen in the stopped-flow spectrophotometer. Flavin oxidation was monitored at 10-nm intervals from 300 to 500 nm. In general, C4a-adduct intermediates (either C4a-hydroperoxyflavin or C4a-hydroxyflavin) have their absorption peaks around 360–400 nm with low absorbance around 450 nm. Therefore, formation and decay of C4a-hydroperoxyflavin and C4a-hydroxyflavin were detected at 360-400 nm, whereas flavin oxidation was monitored at 450-460 nm.

The oxidation of the reduced H213A:3HB complex showed three exponential phases. At the highest oxygen concentration of 0.96 mM (the left-most trace of Fig. 6A), the first phase (0.002 s - 0.023 s) was characterized by an increase in absorbance at 400 nm which was ~76% of the total amplitude change at this wavelength. The observed rate constants for the first phase were linearly dependent on the oxygen concentration with a bimolecular rate constant of $54 \pm 5.5 \times 10^4$ $M^{-1}s^{-1}$ with a significant intercept value of 10.8 ± 3.3 s^{-1} (filled-circles in inset of Fig. 6B). The second phase (0.023 - 0.1 s) was hyperbolically dependent on the oxygen concentration, with the limiting value of 23 ± 3 s^{-1} (open-circles, inset in Fig. 6B). This phase was characterized by an increase in absorbance at 400 nm that was ~ 24% of the total amplitude change at this wavelength. Kinetic analysis of both oxygen-dependent phases indicated the presence of a complex mechanism. The third phase (0.1 - 0.8 s) was independent of oxygen concentration, and gave an observed rate constant of 2 ± 0.02 s^{-1}. When the data observed at 400 nm was analyzed in relation to the increase in absorbance at 453 nm for flavin oxidation (Fig. 6A-B), the first kinetic phase could be interpreted as C4a-intermediate formation, while the second phase is the direct oxidation of reduced enzyme without any C4a-intermediate stabilization. The data also imply that H213A contains mixed populations in which one enzyme fraction reacts faster with oxygen and stabilizes C4a-hydroperoxyflavin, while another one directly oxidizes to the enzyme-bound FAD form.

Simulations of the reaction of H213A were carried out according to the model which describes two enzyme species with different kinetic parameters for the oxygen reaction (H213A:

Fig. 10). The fast population reacts with oxygen to stabilize C4a-hydroperoxyflavin with a rate constant of 4.94 × 10^4 $M^{-1}s^{-1}$ (k_3^{sim}, H213A: Fig. 10, Table 3), whereas the slow population reacts with oxygen with a rate constant of 1.4 × 10^4 $M^{-1}s^{-1}$ (k_6^{sim}, H213A: Fig. 10, Table 3). The simulations were carried out without including the hydroxylation step because the variant did not form the hydroxylated product. The slow population is likely either inactive enzyme that cannot bind 3HB or binds 3HB with a much higher K_d value than the other population. This is because the bimolecular rate constant is similar to the reaction of free reduced enzyme with oxygen (Fig. S5, Supporting Information) and it is not the reaction of free FAD (Fig. 6S, Supporting Information). Although the reaction of free FAD with oxygen is complex [14,15], the observed rate constant of free FAD reacting with 0.13 mM oxygen can be estimated as ~1 s^{-1} [16]. As the observed rate constant of slow population of H213A oxidation is 0.32 s^{-1}, it is clear that this slow phase is not due to oxidation of free FAD. The analysis also indicated that an additional step after C4a-hydroperoxyflavin formation with a rate constant of 15 s^{-1} (k_4^{sim}, H213A: Fig. 10, Table 3) is required before the H_2O_2 elimination step. This step may either be the change in enzyme conformations (from *E-C4a-OOH* to form an active *E*-C4a-OOH* to proceed through the hydroxylation process) or protonation of C4a-OO^- to form C4a-OOH, similar to the wild type enzyme (10). Both enzyme populations can interconvert with forward and reverse rate constants of 5 s^{-1} (k_2^{sim}, H213A: Fig. 10, Table 3) and 4 s^{-1} (k_1^{sim}, H213A: Fig. 10, Table 3), respectively. The kinetic traces from the simulation agree well with those obtained from experimental data (Fig. 10).

Reaction Mechanism of the Reduced H213S:3HB Complex with Oxygen. A solution of the reduced enzyme plus 10 mM 3HB was mixed with buffers containing 10 mM 3HB and various oxygen concentrations in the stopped-flow spectrophotometer. C4a-adduct intermediates were monitored at 405 nm whereas the oxidation of reduced flavin-bound enzyme was monitored at 451 nm (Fig. 7A-B). The oxidation showed four exponential phases. At the highest oxygen concentration of 0.96 mM (the furthest left trace, Fig. 7A), the first phase (0.002 - 0.003 s) was characterized by an increase in absorbance at 405 nm with a small amplitude change at 453 nm (the furthest left trace, Fig. 7B). At the initial time measurement (0.002 s), the absorbance detected was different from the absorbance of the reduced enzyme, indicating that the reaction of the reduced H213S-3HB complex with oxygen occurred during the dead time of the stopped-flow mixing (Fig. 7A). The first phase was dependent on oxygen concentration, with a bimolecular rate constant of 6.5 ± 0.02 × 10^5 $M^{-1}s^{-1}$ (filled-circle line in inset of Fig. 7A, k_3^{exp}, H213S: Fig. 10, Table 3). The second phase

(0.003 - 0.02 s) was the lag phase at 405 nm. Observed rate constants of this phase were linearly dependent on oxygen concentration, and had a bimolecular rate constant of 9.7 ± 0.3 × 10^4 $M^{-1}s^{-1}$ (open-circle line in inset of Fig. 7A, Table 3). This phase occurred in the same time frame as the small increase in absorbance at 453 nm (~15% of the total amplitude change). The third phase (0.02 – 0.3 s) gave an increase in absorbance at 405 nm with a rate constant of 5.8 ± 0.01 s^{-1}. This phase was also observed by an increase in absorbance change at 453 nm (~40% of total amplitude change). The third phase was assigned as the step before hydroxylation because the results from the rapid-quench flow experiments indicated that the hydroxylation occurred during the third phase with an observed rate constant of 1.5 ± 0.2 s^{-1} (open-circle line in Fig. 7B). The fourth phase (0.3 – 3.2 s) was evidenced by a decrease in absorbance at 405 nm with an observed rate constant of 0.48 ± 0.001 s^{-1}. This phase could also be observed as an increase in absorbance at 453 nm (~ 55% of the total amplitude change).

Simulations of the reduced H213S:3HB complex with oxygen were carried out according to the model which describes two enzyme populations that react differently with oxygen. One population reacts with oxygen faster with a bimolecular rate constant of 7.2 × 10^5 $M^{-1}s^{-1}$ (k_3^{sim}, H213S: Fig. 10, Table 3) which is in the same range as the number obtained from experimental data (6.5 ± 0.02 × 10^5 $M^{-1}s^{-1}$, k_3^{exp}, H213S: Fig. 10, Table 3). This population stabilizes a C4a-adduct intermediate. The slower population oxidized without forming the C4a-adduct with a rate constant of 1.1 × 10^5 $M^{-1}s^{-1}$ (k_9^{sim}, H213S: Fig. 10, Table 3) which is in the same range as the number obtained from experimental data (9.7 ± 0.3 × 10^4 $M^{-1}s^{-1}$, k_9^{exp}, H213S: Fig. 10, Table 3). The experimental data (solid lines) agree well with the simulations (dotted-line, Fig. 7).

Data from the simulations suggested that the fast population converts into the slow population, with forward and reverse rate constants of 15 s^{-1} and 1 s^{-1}, respectively (k_2^{sim} and k_1^{sim}, H213S: Fig. 10, Table 3). The bimolecular rate constant of the slow enzyme population reacting with oxygen of 1.1 × 10^5 $M^{-1}s^{-1}$ (k_9^{sim}, H213S: Fig. 10, Table 3) is not the same as that of free enzyme oxidation (Fig. S5, Supporting Information). Therefore, the slow species is not the free enzyme, but rather, both fast and slow species are H213S:3HB complexes. The fast population reacts with oxygen forming a C4a-adduct with a bimolecular rate constant of 7.2 × 10^5 $M^{-1}s^{-1}$ (k_3^{sim}, H213S: Fig. 10, Table 3). The simulation also identified another step after C4a-adduct formation with a rate constant of 5.9 s^{-1} (k_4^{sim}, H213S: Fig. 10, Table 3) and an uncoupling path of C4a-

hydroperoxyflavin elimination with rate of 0.9 s^{-1} (k_5^{sim}, H213: Fig. 10, Table 3). This step may be the protonation of the peroxy group from C4a-OO^- to C4a-OOH similar to the wild type enzyme (10). According to the simulations, the fast population of C4a-hydroperoxyflavin hydroxylates the substrate with an observed rate constant of 0.9 s^{-1}, which is the combination of the hydroxylation rate constant of 0.3 s^{-1} (k_H in Table 2 or k_6^{sim}, H213S: Fig. 10) and the hydrogen peroxide elimination rate constant of 0.6 s^{-1} (k_e, in Table 2 or k_7^{sim} H213S: Fig. 10). Based on simulations with a starting enzyme concentration of 24.6 μM, 5.99 μM product (24% yield) should be obtained. This value is close to the percentage of product formation obtained from single turnover experiments of 28% (Table 2), validating the model described in Fig. 10. It was necessary to include the uncoupling step (k_5^{sim}, H213S: Fig. 10) in the reaction scheme because removal of this step would result in product formation in different value (42%). For the next step consisting of dehydration of C4a-hydroxyflavin to return to the oxidized FAD state, the simulations yielded the rate constant of 0.41 s^{-1} (k_8^{sim}, H213S: Fig. 10, Table 3) which is similar to the value obtained from experimental data (0.48 $\pm$ 0.001 s^{-1}, k_8^{exp}, H213S: Fig. 10, Table 3).

Kinetics of the Reaction of the Reduced H213E:3HB complex with Oxygen. A solution of the reduced enzyme plus 10 mM 3HB was mixed with buffers containing 10 mM 3HB and various concentrations of oxygen in the stopped-flow spectrophotometer. The results showed three observed phases. At the highest oxygen concentration of 0.96 mM (the left-most trace in Fig. 8), the first phase (0.002 - 0.003) was characterized by an increase in absorbance at 380 nm with a small absorbance increase at 452 nm. As the absorbance detected at 0.002 s was different from the absorbance of the reduced enzyme, it suggested that some part of the reaction of the reduced enzyme H213E-3HB complex with oxygen occurred during the dead time of the stopped-flow mixing. The first phase was dependent on oxygen concentration, with a bimolecular rate constant of 1.3 $\pm$ 0.02 $\times$ 10^6 $M^{-1}s^{-1}$ (inset in Fig. 8A). The second phase (0.003 - 0.13 s) showed increase of rate constant at higher oxygen concentrations, resulting in a large increase in absorbance at 452 nm (~78% of the total amplitude change). However, the amplitude of this phase at 452 nm was not large enough to be analyzed for accurate observed rate constants, especially at the low oxygen concentrations (0.13 and 0.31 mM). At the highest oxygen concentration of 0.96 mM, the observed rate constant of this phase was 23.6 $\pm$ 0.3 s^{-1}. The third phase (0.13 - 12 s) was characterized by an increase in absorbance at both 380 nm and 452 nm (~20% of the total amplitude change) with

a rate constant of 0.14 ± 0.01s^{-1}. As the data from rapid quench analysis indicated that the hydroxylation rate constant was 35 ± 2 s^{-1} (open-circle line in Fig. 8B), and that the substrate hydroxylation occurred during the second observed phase.

Simulations for the reaction of the reduced H213E:3HB complex were carried out according to the model describing two enzyme populations reacting with oxygen. Data from simulations (dotted lines) agree well with the observed kinetic traces (solid lines) (Fig. 8A-B). The fast population reacts with oxygen to form the C4a-hydroperoxyflavin with a bimolecular rate constant of 1.4 × 10^6 $M^{-1}s^{-1}$ (k_3^{sim}, H213E: Fig. 10, Table 3) which is in the same range as the observed data (k_3^{exp}, 1.3 ± 0.02 × 10^6 $M^{-1}s^{-1}$, Table 3). The slow population oxidized without forming the C4a-adduct with a rate constant of 5 × 10^3 $M^{-1}s^{-1}$ (k_7^{sim}, H213E: Fig. 10, Table 3). According to the simulation analysis, the fast population interconverts into the slow population with forward and reverse rate constants of 30 s^{-1} and 7 s^{-1}, respectively (k_2^{sim} and k_1^{sim}, H213E: Fig. 10, Table 3). The simulation identified another step with a rate constant of 75 s^{-1} (k_4^{sim}, H213E: Fig. 10, Table 3) following the formation of the C4a-adduct, which correlated with a small increase in absorbance at 380 nm (0.003-0.02 s in the kinetic trace at 0.96 mM oxygen, Fig. 8A). This step may be the change in enzyme conformations (from *E-C4a-OOH* to an active E^**-C4a-OOH* that is required for hydroxylation) or the protonation of the peroxy group of C4a-OO^- to form C4a-OOH, similar to the step that occurs in the wild type enzyme [10]. The hydroxylation rate constant obtained from simulation was 35 s^{-1} (k_5^{sim}, H213E: Fig. 10, Table 3). After hydroxylation, the enzyme rapidly dehydrates and returns to the oxidized state without stabilizing C4a-hydroxyflavin. This step was consistent with the second kinetic phase in which the absorbance at 380 nm and 450 nm increased and most of the enzyme was in the oxidized form. Based on simulation and the model shown in Fig. 10 (H213E), a percentage yield of product of 98.6% (22 μM) should be obtained from a starting concentration of reduced enzyme of 22.3 μM, which is consistent with the results obtained from the single turnover experiment (product of ~92%, Table 2). The kinetic traces showed a small fraction of enzyme (less than 10 %) slowly returning to the oxidized state with a rate constant of 0.13 s^{-1} (k_6^{sim} of H231E) calculated from the simulation or 0.14 ± 0.01 s^{-1} (k_6^{exp} of H213E, Fig. 10, Table 3) obtained from the experimental results. As this step is much slower than the k_{cat} of this variant (5.11 s^{-1}, Table 2), the data imply that this step is not involved in catalysis and may reflect a fraction of inactive enzyme.

Kinetics of the Reaction of the Reduced H213D:3HB complex with Oxygen. A solution of reduced H213D plus 10 mM 3HB was mixed with buffers containing 10 mM 3HB and various concentrations of oxygen in the stopped-flow spectrophotometer. The kinetic traces showed three observable phases. At the highest oxygen concentration of 0.96 mM (the left-most trace in Fig. 9), the first phase (0.002 - 0.005) was characterized by an increase in absorbance at 405 nm without any significant change at 451 nm. The absorbance detected at 0.002 s was different from the absorbance of the reduced enzyme, indicating that some part of the reaction occurred during the dead time of the stopped-flow mixing. The first phase was dependent on oxygen concentration with a bimolecular rate constant of 4.46 $\pm$ 0.03$\times 10^5$ $M^{-1}s^{-1}$ (inset in Fig. 9A). As an absorbance change around the 451 nm region was not observed for this phase, this phase likely represents the formation of C4a-hydroperoxyflavin. The second phase (0.005 - 1 s) showed an increase in absorbance at 405 nm with observed rate constants of 1.54 s^{-1}, 1.82 s^{-1}, 2.71 s^{-1} and 3.41 s^{-1}, for the reaction at oxygen concentrations of 0.13 mM, 0.31 mM, 0.61 mM and 0.96 mM, respectively. This phase also showed an increase in absorbance at 452 nm (~61% of the total amplitude change, Fig. 9B). The data from the rapid-quench flow experiments indicated that the product was formed with a rate constant of 0.63 $\pm$ 0.05 s^{-1} (open-circle line in Fig. 9B), implying that the hydroxylation occurred during the second phase that was observed by the stopped-flow experiments. The third phase (1 - 5 s) was a decay of the C4a-adduct to form the oxidized enzyme, as it showed a decrease in absorbance at 405 nm and an increase at 452 nm (~40% of the total amplitude change) with a rate constant of 0.34 s^{-1} (Fig. 9B).

Simulations of the reaction of the H213D:3HB complex with oxygen were carried out according to a model describing two enzyme populations reacting with oxygen. Results from the simulations (dotted lines) agree well with the experimental data (solid lines, Fig. 9A-B). The fast population formed C4a-hydroperoxyflavin with a bimolecular rate constant of 4.5 $\times$ 10^5 $M^{-1}s^{-1}$ (k_3^{sim}, H213D: Fig. 10, Table 3) which is similar to the results obtained from experimental data (4.4 $\pm$ 0.03 $\times$ 10^5 $M^{-1}s^{-1}$, k_3^{exp}, H213D: Fig. 10, Table 3). The slow population oxidized without forming a C4a-adduct with a rate constant of 170 $M^{-1}s^{-1}$ (k_8^{sim}, H213D: Fig. 10, Table 3). This flavin oxidation rate was even slower than the re-oxidation rate for the free enzyme 2.1 $\times$ 10^3 $M^{-1}s^{-1}$ (Fig. S6, Supporting Information), indicating that the slow oxidation is not attributed to oxidation of the free enzyme species.

The model in Fig. 10 also indicates that the fast enzyme population can be converted into the slow population with forward and reverse rate constants of 87 s^{-1} and 3 s^{-1}, respectively (k_2^{sim} and k_1^{sim}, H213D: Fig. 10, Table 3). Only the fast population reacts with oxygen to form the C4a-hydroperoxyflavin. The simulation also identified a step with a rate constant of 2.8 s^{-1} (k_4^{sim}, H213D: Fig. 10, Table 3). This step may either be the change in enzyme conformations (from *E-C4a-OOH* to a more active E^**-C4a-OOH* to proceed through hydroxylation) or the protonation of C4a-OO^- to form C4a-OOH, similar to the wild-type enzyme [10]. The hydroxylation occurred at the following step with a rate constant of 0.65 s^{-1} (k_H in Table 2 or k_5 in H213D: Fig. 10, Table 3). The elimination of hydrogen peroxide which was not coupled with hydroxylation also occurred with a rate constant of 0.45 s^{-1} (k_e in Table 2 or k_6 in H213D: Fig. 10, Table 3). Simulations according to the model described in Fig. 10 suggest that a product yield of 58.6% (15.3 μM) should be obtained from a starting concentration of reduced enzyme of 26.1 μM. This number agrees well with the results from the single turnover experiment which gave a product yield of 52% (Table 2). After hydroxylation, the C4a-hydroxyflavin intermediate underwent dehydration to form the oxidized enzyme with a rate constant of 0.35 s^{-1} obtained by simulation (k_7^{sim}, H213D: Fig. 10, Table 3) which is similar to the actual observed rate constant of 0.45 s^{-1} (k_7^{exp}, H213D: Fig. 10, Table 3).

DISSCUSSION

Our investigation of 3HB6H active site variants using transient kinetics (stopped-flow and rapid quench flow techniques), product analysis and ligand binding studies have shown that Tyr217 is important for substrate binding, while His213 is crucial for substrate hydroxylation. The results from the product analysis studies also indicated that 3HB6H is highly selective for the *para*-hydroxylation reaction because active variants only formed 2,5-DHB as a product. Details of the analysis have revealed insight into the reaction mechanism of how the active site residues of 3HB6H control the efficiency and regioselectivity of substrate hydroxylation.

The substitution of Tyr217 with residues that cannot make a hydrogen-bond interaction with the carboxylate group of 3HB such as Phe (Y217F) and Ala (Y217A) resulted in a substantial decrease or complete abolishment of substrate binding. For Y217S in which the side chain can still maintain a hydrogen bond interaction with the carboxylate group of the substrate, the substrate binding ability was retained, but displayed a very high K_d value (Fig. S1, Supporting Information). These results suggest that a proper distance between the side chain of residue 217 and the

carboxylate group of 3HB is required for making a suitable anchoring point for substrate binding. However, substitution of His213 with residues with different properties did not significantly affect the enzyme binding affinity for 3HB. In fact, H213E showed the hightest binding affinity (K_d = 0.052 mM, Table 2), which was 3-fold stronger than the binding affinity of the wild-type enzyme (K_d = 0.15 mM, Table 2). Interestingly, the K_d of substrate binding for H213D (0.35 mM, Table 2), which has the same negative charge as H213E, is 7-fold higher than that of H213E. These results indicate that a proper distance between residue 213 and 3HB are required for optimal substrate interaction, thus maximizing the substrate binding affinity. The kinetics of H213S binding showed that the spectral perturbation of FAD upon 3HB binding occurred during the dead time (less than 0.002 s, Fig. 4), which is the fastest among H213 mutants and wild-type enzyme [12]. This distinctive binding property in H213S implies that dynamics of ligand binding in this variant may be different from other enzymes.

Studies of His213 variants (H213A, H213S, H213E and H213D) indicated that the interaction between the 3-OH of 3HB and His213 is crucial for substrate hydroxylation because the H213A variant could not perform hydroxylation, while the hydroxylation efficiency for H213S and H213D was decreased to 28% and 52%, respectively. Among all of the variants investigated, the H213E variant displayed the most distinctive properties that were useful for providing insight into the reaction mechanism of 3HB6H. This variant had a hydroxylation yield of 92%, which is higher than the wild-type enzyme (86%). The hydroxylation rate constants of H213E and WT 3HB6H are comparable (35 s^{-1} and 36 s^{-1}). When His213 was replaced by Glu *in silico* (Fig. S7, Supporting Information), the putative distance between 3HB and Glu213 or His213 are quite similar, ~3.5 Å and ~3.4 Å, respectively. As the H213D has a hydroxylation efficiency of 50%, which is much lower than the value for H213E, the data suggest that not only the ionic interaction between the 3-OH group of 3HB and residue 213, but also the proper distance between these groups is required to achieve efficient hydroxylation.

The hydroxylation mechanism of 3HB6H likely occurs via electrophilic aromatic substitution (Fig. 11). For H213E, the carboxylate group of Glu213 may facilitate the deprotonation of the hydroxyl group of 3HB (Fig. 11A). Based on difference spectra experiments (Fig. 5), H213E probably binds 3HB in the phenolic form because the spectrum of enzyme-3HB showed a peak around 288 nm which is similar to the absorption peak of free 3HB at pH 8.0. However, no peak was observed at 312 nm, which is the peak of free 3HB at pH 12.0. This result implies that His in

the wild-type enzyme may also bind the substrate in the phenolic form. We propose that the phenolic proton may be shared between the 3-OH group of 3HB and the carboxylate group of Glu213. The proton may shift over to Glu213 (or His213) during the base abstraction process to facilitate the formation of the transition state and then is transferred back to the substrate during the rearomatization step (Fig. 11). These results for H213E suggest that a negative charge at position 213 can enable hydroxylation. Since the H213D variant does not have the same hydroxylation efficiency as H213E, this implies that not only a negative charge, but also a proper distance between residue 213 and the 3-OH group of the substrate is required, presumably so that the deprotonation is facilitated. For the wild-type enzyme, His213 may have a similar function as Glu213 in the His213Glu variant. A similar type of catalytic residue was proposed for 3-hydroxybenzoate 4-hydroxylase from *Comamonas testosterone* in that Asp75 acts as a catalytic base to abstract a proton from 3-hydroxybenzoate [17] similar to the reactions of H213D and H213E variants of 3HB6H. The hydroxylation mechanism of H213S may be different from the reactions of the wild-type enzyme and the other variants. Based on the x-ray structure of 3HB6H [11], it is possible that Ser213 in this variant can form a hydrogen bond network with His366 and Ser213 and help deprotonate the hydroxyl group of 3HB. For the wild-type enzyme, we propose that His213 interacts with the 3-OH moiety of 3HB and acts as a catalytic base to deprotonate 3-OH so that the electrophilic aromatic substitution can readily occur (Fig.11B).

Deprotonation of the phenolic group in flavoenzyme active sites is an important mechanism to enhance the nucleophilicity of the aromatic substrate prior to the hydroxyl group transfer from the C4a-hydroperoxyflavin electrophile [18]. Different enzymes in Group A flavoprotein monooxygenases have different specificities in substrate form selectivity. In 4-hydroxybenzoate 3-hydroxylase (PHBH), deprotonation of *para*-hydroxybenzoate (*p*OHB) to form the phenolate substrate is controlled by a hydrogen bond network [19,20] that is composed of two tyrosines, two water molecules and a histidine which acts to transfer the phenolic proton to the outside solvent [21]. For 2-methyl-3-hydroxypyridine-5-carboxylate (MHPC)-monooxygenase (MHPCO), the enzyme selectively binds MHPC in the tripolar ionic form in which the 3-OH is deprotonated [22,23]. The interaction between MHPC, Tyr82 and Tyr223 and the water molecules surrounding the substrate binding are crucial for the selectivity of the proper ionic form of substrate [24]. The active site of 3HB6H is rather hydrophobic when compared to those of PHBH and MHPCO. Substrate deprotonation in these enzymes involves hydrogen bond networking with water molecules in their

active sites [21,24,25] while the deprotonation of 3-OH in 3HB6H likely occurs via a direct interaction with His213 during hydroxylation. In contrast to 2,6-dihydroxypyridine-3-hydroxylase from *Arthrobacter nicotinovorans* which can catalyze para-hydroxylation as in 3HB6H, the active site contains water molecule interacting with His202 and His314. Both residues are proposed to deprotonate the 6-OH of the aromatic substrate for C3 hydroxylation [26]. The functional role of an active site His in the deprotonation of the hydroxyl group of a phenolic substrate has also been found in another group of flavoproteins monoxygenase such as in the oxygenase component (C_2) of *p*-hydroxyphenylacetate hydroxylase from *Acinetobactor baumannii*. In C_2, His120 is closely located to the 4-OH group of *p*-hydroxyphenylacetate, and changing this residue to other types rather than a positively charged residue impairs the hydroxylation activity [27].

The proper anchoring point is not only crucial for the ligand binding interaction but also crucial for the proper geometric selectivity found in the *ortho*- or *para*-hydroxylation enzymes. Comparison of the substrate binding geometry in 3HB6H (*para*-hydroxylation), PHBH (*ortho*-hydroxylation), and 3HB4H (*ortho*-hydroxylation) indicates that all of these hydroxylases position their substrates such that the putative hydroxylation site is closest to the C4a-position of FAD (Fig. S8, Supporting information). This structural feature is key for achieving the regioselectivity of these enzymes. The role of Tyr217 as the substrate anchoring point is equivalent to Arg214 in PHBH, which provides an interaction with the carboxylate group of the *p*OHB substrate. Replacing these residues with others that lack this hydrophilic interaction resulted in the variants that had abolished substrate binding ability [28-30].

In conclusion, this study has illustrated the functional role of the active site residues Tyr217 and His213 in the reaction of 3HB6H from *R. jostii* RHA1. The results clearly show that Tyr217 is crucial for substrate binding and His213 for substrate hydroxylation. The change of His213 into Glu resulted in a fully active hydroxylase with the highest efficiency in substrate hydroxylation. This is remarkable from an evolutionary point of view considering the fact that His213, like Tyr217, is strictly conserved in all 3HB6H sequences reported thus far. However, as the wild-type enzyme is more stable than the His213Glu variant, it implies that both catalytic efficiency and protein stability need to be considered from an evolutionary perspective. All 3HB6H variants are specific for *para*-hydroxylation, supporting that the 3HB6H active site scaffold is robust for *para*-hydroxylation of a phenolic compound.

ACKNOWLEDGMENT

This work was supported by The Thailand Research Fund through grants No. RSA5580050 (to J.S.), No. RTA5680001 (to P.C.) and No. MRG5680043 (to D.P.), and Mahidol University Research Grant 2558A11003398 (to D.P.), Chulalongkorn University through the Ratchadaphiseksomphot Endowment Fund, and the Faculty of Dentistry, Chulalongkorn University (to J.S.), and the Faculty of Science, Mahidol University (to P.C.), and the Graduate School VLAG, Wageningen, The Netherlands (to W.v.B.). We also thank Barrie Entsch for critical reading of the manuscript.

REFERENCES

1. Gupta S, Pathak B & Fulekar MH (2015) Molecular approaches for biodegradation of polycyclic aromatic hydrocarbon compounds: a review. *Rev Environ Sci Biotechnol 14*, 241-269.

2. Krastanov A, Alexieva Z & Yemendzhiev H (2013) Microbial degradation of phenol and phenolic derivatives. *Eng Life Sci 13*, 76–87.

3. Martínková L, Uhnáková B, Pátek M, Nešvera J & Kř̆en V (2009) Biodegradation potential of the genus *Rhodococcus*. *Environ Int 35*, 162–177.

4. de Carvalho CC, Costa SS, Fernandes P, Couto I & Viveiros M (2014) Membrane transport systems and the biodegradation potential and pathogenicity of genus *Rhodococcus*. *Front Physiol 133*, eCollection.

5. Lang S & Philp JC (1998) Surface-active lipids in *Rhodococci. Antonie Van Leeuwenhoek 74*, 59–70.

6. Kirk TK & Farrell RL (1987) Enzymatic "combustion": the microbial degradation of lignin. *Annu Rev Microbiol 41*, 465-505.

7. Diaz E (2004) Bacterial degradation of aromatic pollutants: a paradigm of metabolic versatility, *Int. Microbiol.* 7, 173–180.

8. Montersino S & van Berkel WJ (2012) Functional annotation and characterization of 3-hydroxybenzoate 6-hydroxylase from *Rhodococcus jostii* RHA1. *Biochim Biophys Acta 1824*, 433-442.

9. Huijbers MM, Montersino S, Westphal AH, Tischler D & van Berkel WJ (2014) Flavin dependent monooxygenases. *Arch Biochem Biophys 544*, 2-17.

10. Sucharitakul J, Tongsook C, Pakotiprapha D, van Berkel WJ & Chaiyen P (2013) The reaction kinetics of 3-hydroxybenzoate 6-hydroxylase from *Rhodococcus jostii* RHA1 provide an understanding of the para-hydroxylation enzyme catalytic cycle. *J Biol Chem 288*, 35210-35221.

11. Montersino S, Orru R, Barendregt A, Westphal AH, van Duijn E, Mattevi A & van Berkel WJ (2013) Crystal structure of 3-hydroxybenzoate 6-hydroxylase uncovers lipid-assisted flavoprotein strategy for regioselective aromatic hydroxylation. *J Biol Chem 288*, 26235-26245.

12. Sucharitakul J, Wongnate T, Montersino S, van Berkel WJ & Chaiyen P (2012) Reduction kinetics of 3-hydroxybenzoate 6-hydroxylase from *Rhodococcus jostii* RHA1. *Biochemistry 51*, 4309-4321.

13. Ellis KJ & Morrison JF (1982) Buffers of constant ionic strength for studying pH-dependent processes. *Meth Enzymol 87*, 405-26.

14. Bruice TC (1984) Oxygen-flavin chemistry. *Isr J Chem 24*, 54-61.

15. Massey V, Strickland S, Mayhew SG, Howell LG, Engel PC, Matthews RG, Schuman M & Sullivan PA (1969) The production of superoxide anion radicals in the reaction of reduced flavins and flavoproteins with molecular oxygen. *Biochem Biophys Res Commun 36*, 891-897.

16. Sucharitakul J, Phongsak T, Entsch B, Svasti J, Chaiyen P & Ballou DP (2007) Kinetics of a two-component *p*-hydroxyphenylacetate hydroxylase explain how reduced flavin is transferred from the reductase to the oxygenase. *Biochemistry 46*, 8611−8623.

17. Hiromoto T, Fujiwara S, Hosokawa K & Yamaguchi H (2006) Crystal structure of 3-hydroxybenzoate hydroxylase from *Comamonas testosteroni* has a large tunnel for substrate and oxygen access to the active site. *J Mol Biol 364*, 878-896.

18. Palfey BA & McDonald CA (2010) Control of catalysis in flavin-dependent monooxygenases. *Arch Biochem Biophys 493*, 26-36.

19. Entsch B, Palfey B A, Ballou D P & Massey V (1991) Catalytic function of tyrosine residues in *p*-hydroxybenzoate hydroxylase as determined by the study of site-directed mutants. *J Biol Chem 266*, 17341-17349.

20. Palfey BA, Entsch B, Ballou, DP & Massey V (1994) Changes in the catalytic properties of *p*-hydroxybenzoate hydroxylase caused by the mutation Asn300Asp. *Biochemistry 33*, 1545-1554.
21. Frederick KK & Palfey BA (2005) Kinetics of proton-linked flavin conformational changes in *p*-hydroxybenzoate hydroxylase. *Biochemistry 44*, 13304-13314.
22. Chaiyen P, Brissette P, Ballou DP & Massey V (1997) Reaction of 2-methyl-3-hydroxypyridine-5-carboxylic acid (MHPC) oxygenase with N-methyl-5-hydroxynicotinic acid: studies on the mode of binding, and protonation status of the substrate. *Biochemistry 36*, 13856-13864.
23. Chaiyen P (2010) Flavoenzymes catalyzing oxidative aromatic ring-cleavage reactions. *Arch Biochem Biophys 493*, 62-70.
24. Luanloet T, Sucharitakul J & Chaiyen P (2015) Selectivity of substrate binding and ionization of 2-methyl-3-hydroxypyridine-5-carboxylic acid oxygenase. *FEBS J*, doi: 10.1111/febs.13220.
25. Frederick KK, Ballou DP & Palfey BA (2001) Protein dynamics control proton transfers to the substrate on the His72Asn mutant of *p*-hydroxybenzoate hydroxylase. *Biochemistry 40*, 3891-3899.
26. Treiber N, & Schulz GE (2008) Structure of 2,6-dihydroxypyridine 3-hydroxylase from a nicotine-degrading pathway. *J Mol Biol 379*, 94-104.
27. Tongsook C, Sucharitakul J, Thotsaporn K & Chaiyen P (2011) Interactions with the substrate phenolic group are essential for hydroxylation by the oxygenase component of *p*-hydroxyphenylacetate 3-hydroxylase. *J Biol Chem 286*, 44491-44502.
28. van Berkel WJ, Westphal A, Eschrich K, Eppink M & de Kok A (1992) Substitution of Arg214 at the substrate-binding site of *p*-hydroxybenzoate hydroxylase from *Pseudomonas fluorescens*. *Eur J Biochem 210*, 411-419.
29. Schreuder HA, Mattevi A, Obmolova G, Kalk KH, Hol WG, van der Bolt FJ & van Berkel WJ (1994) Crystal structures of wild-type *p*-hydroxybenzoate hydroxylase complexed with 4-aminobenzoate,2,4-dihydroxybenzoate, and 2-hydroxy-4-aminobenzoate and of the Tyr222Ala mutant complexed with 2-hydroxy-4-aminobenzoate. Evidence for a proton channel and a new binding mode of the flavin ring. *Biochemistry 33*, 10161-10170.
30. van der Bolt FJ, Vervoort J & van Berkel WJ (1996) Flavin motion in *p*-hydroxybenzoate hydroxylase. Substrate and effector specificity of the Tyr22-->Ala mutant. *Eur J Biochem 237*, 592-600.

Table 1. Molar absorption coefficients of 3HB6H variants and kinetic and thermodynamic parameters for the binding of 3HB.

3HB6H	λ_{max}	ε ($M^{-1}cm^{-1}$)	K_d (mM)[b] (25 °C)	k_f^{sim} ($M^{-1}s^{-1}$)[d] (4 °C)	k_r^{sim} (s^{-1})[d] (4 °C)	K_d (mM) (4 °C)
WT[a]	452	11 ± 0.03	0.15 ± 0.02	4×10^5	64	0.16
H213A	453	11.2 ± 0.02	0.12 ± 0.015	1.72×10^6	70	0.041
H213S	451	11.2 ± 0.05	0.72 ± 0.05	very fast[e]	very fast[e]	0.42[f]
H213E	452	11.2 ± 0.08	0.052 ± 0.004	1.04×10^6	70	0.067
H213D	451	11 ± 0.03	0.35 ± 0.03	3.1×10^5	117	0.38
Y217A	450	11.1 ± 0.04	very high	—	—	—
Y217F	450	11.4 ± 0.01	~7.5[c]	—	—	—
Y217S	452	11.4 ± 0.12	very high	—	—	—

[a]Data from reference [12]
[b]Data from static titration of 3HB to oxidized enzyme (supporting information)
[c]K_d from Fig. S1, Supporting Information.
[d]k_f is for 3HB binding to oxidized enzyme, and k_r is for 3HB dissociation from oxidized enzyme.
[e]The absorbance change due to binding of 3HB to the oxidized enzyme occurred during the dead time of the stopped-flow spectrophotometer.

[f] K_d for H213S:3HB complex was calculated from a plot of absorbance change after the dead time (Fig. 4).

Table 2. Product formation from single-turnover reactions and rate constants of product formation. The reaction was performed in 100 mM sodium phosphate and 100 mM sodium sulfate pH 8.0 at 4 °C. The percentage of product coupling was calculated from the ratio of product formed to the total amount of reduced enzyme. Rate constants of product formation were measured by rapid quench flow experiments.

Enzymes	Product formation (%)	k_{obs} [b] (s^{-1})	k_H [c] (s^{-1})	k_e [c] (s^{-1})
WT	86[a]		36[a]	13[a]
H213A	0	—	—	1.9
H213S	28 ± 5	1.5 ± 0.2	0.3	0.6
H213E	92 ± 6	35 ± 2	35	—
H213D	52 ± 7	0.63 ± 0.05	0.65	0.45
Y217A	4.6 ± 1[d]	—	—	—
Y217F	3.3 ± 2[d]	—	—	—
Y217S	3.7 ± 3[d]	—	—	—

[a] Data from reference [10].
[b] k_{obs} (s^{-1}): observed rate constants for product forming obtained from rapid-quench flow at oxygen concentration ~0.13 mM O_2 (air saturation before mixing).

[c]The rate constants of k_H (rate of hydroxylation) and k_e (rate of hydroxgen peroxide elimination) obtained from simulation according to reaction models in Fig. 10.
[d]The product was detected by HPLC separation with a small absorbance signal at 320 nm.

Table 3. Rate constants of the oxidative half-reactions of reduced His213 variant-3HB complexes obtained from the experimental data and simulations.

Rate constants	WT	H213A	H213S	H213E	H213D
k_1^{sim}	—	4 s^{-1}	1 s^{-1}	7 s^{-1}	3 s^{-1}
k_2^{sim}	—	5 s^{-1}	15 s^{-1}	30 s^{-1}	87 s^{-1}
k_3^{sim}	1.6 × 10^{6a}	4.94 × 10^{4b}	7.2 × 10^{6b}	1.4 × 10^{6b}	4.5 × 10^{6b}
k_3^{exp}		—	6.5 ± 0.02 × 10^{5b}	1.3 ± 0.02 × 10^{6b}	4.46 ± 0.03×10^{5b}
k_4^{sim}		15 s^{-1}	5.9 s^{-1}	75 s^{-1}	2.8 s^{-1}
k_4^{exp}	—	—	—	—	—
k_5^{sim}	—	2 s^{-1}	0.9 s^{-1}	35 s^{-1}	0.65 s^{-1}
k_5^{exp}		2 ± 0.02 s^{-1}	—	—	—
k_6^{sim}	—	1.4 × 10^{4b}	0.3 s^{-1}	0.13 s^{-1}	0.45 s^{-1}
k_6^{exp}	—	—	—	0.14 ± 0.01s^{-1}	—
k_7^{sim}	—	—	0.6 s^{-1}	5 × 10^{6b}	0.35 s^{-1}
k_7^{exp}		—	—	5.59 ± 0.27 × 10^{3b}	0.45 s^{-1}
k_8^{sim}	—	—	041 s^{-1}	—	170[b]
k_8^{exp}	—	—	0.48 ± 0.001 s^{-1}	—	—
k_9^{sim}	—	—	1.1 × 10^{6b}	—	—
k_9^{exp}	—	—	9.7 ± 0.3 × 10^{4b}	—	—
$k_{cat(app)}$	6.55 s^{-1}[a]	1.2 ± 0.01 s^{-1}[c]	1.34 ± 0.05 s^{-1}[d]	5.11 ± 0.14 s^{-1}[d]	0.44 ± 0.15 s^{-1}[d]

[exp]Rate constants obtained from experiments.
[sim]Rate constants obtained from simulations.
[a]Data from reference [10].
[b]Bimolecular rate constant ($M^{-1}s^{-1}$).
[c]Apparent catalytic constant (k_{cat}) obtained from steady-state assays monitored by NADH consumption at 395 nm. The reaction contained H213A (5 μM), 1 mM NADH, 10 mM 3HB and

oxygen (after mixing concentrations). The reaction was performed in 100 mM sodium phosphate and 100 mM sodium sulfate pH 8.0 at 4 ^{o}C.
[d]Apparent catalytic constant (k_{cat}) obtained from enzyme monitored turnovers (see Experimental Procedures).

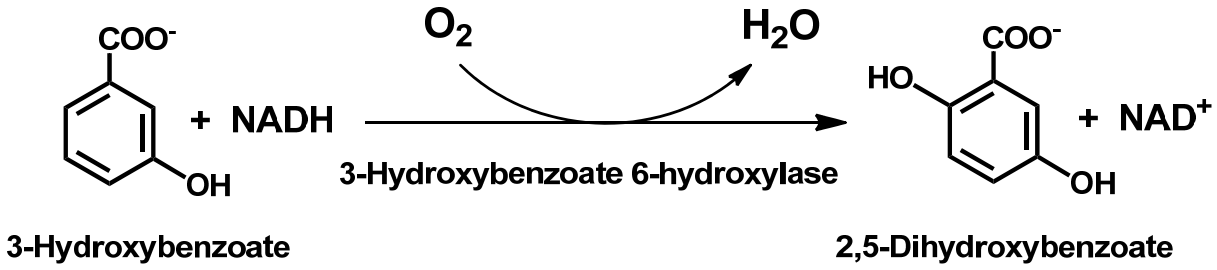

Figure 1. The overall reaction of 3-hydroxybenzoate 6-hydroxylase (3HB6H).

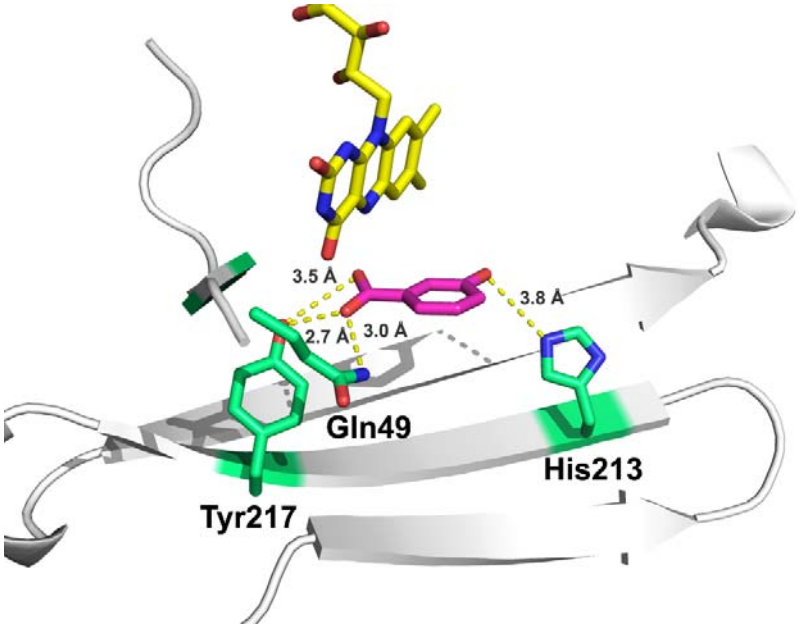

Figure 2. The active site structure of the 3HB6H:3HB complex. Based on the structure of the H213S variant (PDB entry 4BK1), residue His213 was modeled by replacing Ser213. The dotted lines represent interactions between His213, Tyr217 and Gln49 with 3HB. Numbers indicate distances in angstroms.

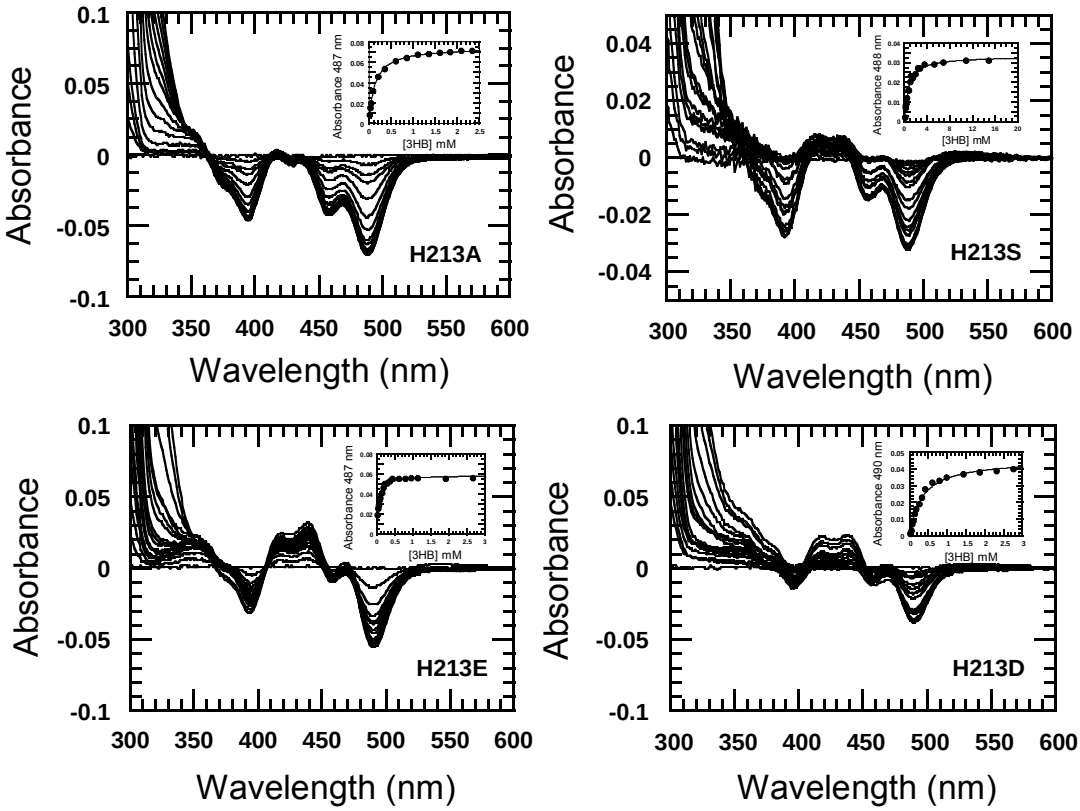
Absorbance
Wavelength (nm)
H213A
Absorbance 487 nm
[3HB] mM
H213S
Absorbance 488 nm
[3HB] mM
H213E
Absorbance 487 nm
[3HB] mM
H213D
Absorbance 490 nm
[3HB] mM

Figure 3. Binding of 3HB and the oxidized 3HB6H variants H213A, H213S, H213E and H213D. Solutions of free enzymes (~ 27 μM) in 100 mM sodium phosphate and sodium sulfate pH 8.0 at 25 °C were placed in both reference and sample cuvettes. The enzyme in the sample cuvette was titrated with 3HB solution, while an equal volume of buffer was added to the enzyme solution in the reference cuvette. The difference absorption spectra were recorded from 300-600 nm. The absorption changes at 487 nm for both H213A and H213E, at 488 nm for H213S, and at 490 nm for H213D were plotted against various 3HB concentrations (inset figures).

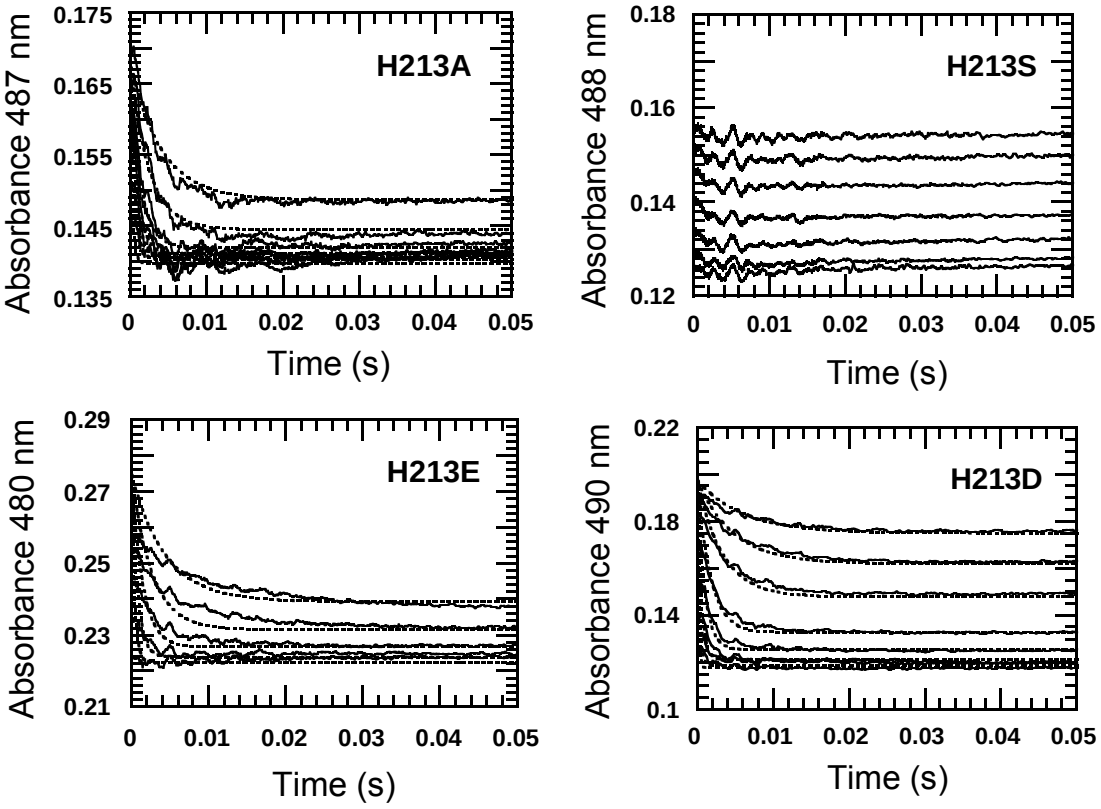

Figure 4. Kinetics of 3HB binding to the His213 variants. A solution of oxidized enzyme (~30 μM) was mixed with buffer containing various concentrations of 3HB in the stopped-flow

spectrophotometer. The lowest to highest concentrations, H213A: 0.1, 0.2, 0.4, 0.6 0.8, 1, 2 mM, H213S: 0.1, 0.2, 0.4, 0.8, 2, 4, 8 mM, H213E: 0.15, 0.3, 0.6 1.2, 2.4 mM, H213D: 0.15, 0.3, 0.6, 1.5, 3, 6, 12. 24 mM are shown as upper to lower traces. All concentrations as described were after mixing. The reactions were monitored at wavelengths showing maximal absorbance changes due to spectral perturbation from substrate binding (cf. Fig. 3).

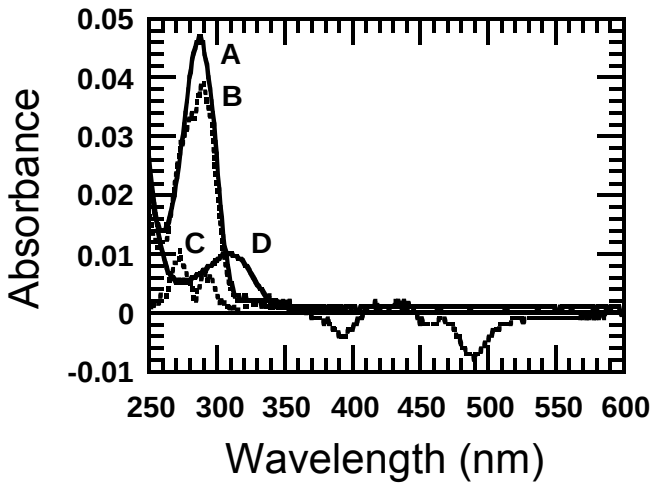

Figure 5. Identification of 3HB bound to 3HB6H. The experiments were performed in a double-beam spectrophotometer. The solid line is a baseline in which free H213E (15 μM) in the three-buffer system pH 8.0 (100 mM ACES + 100 mM Tris H_2SO_4 + 100 mM ethanolamine + 100 mM sodium sulfate) was placed in both sample and reference cells. Spectrum A (solid line) was recorded when the sample cell contained free 3HB (20 μM) in the three-buffer system pH 8.0. Spectrum B (dotted line) was recorded when the sample cell contained 15 μM enzyme and 20 μM 3HB in the three-buffer system pH 8.0 and the reference cell contained only 15 μM of free enzyme in the same buffer. Spectrum C (dotted line) is obtained by subtraction of the spectrum of 16.4 μM

free 3HB from spectrum B in the same pH buffer to calculate the spectrum of enzyme-bound 3HB of 3.6 μM. Spectrum D (solid line) is a spectrum of the phenolate form of 3HB (3.6 μM) in the three-buffer system at pH 12.

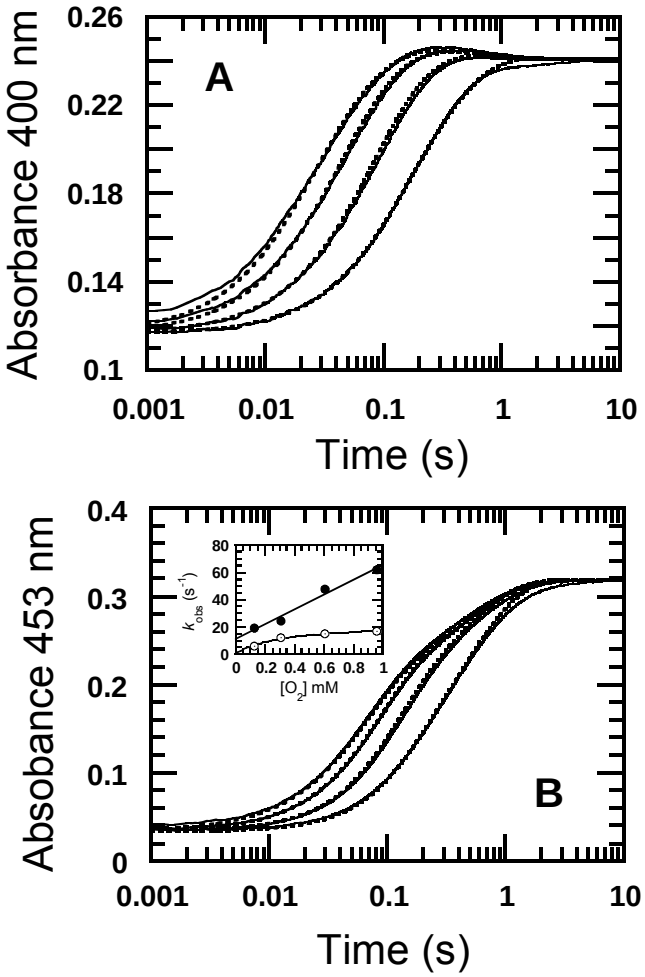

Figure 6. Reaction of reduced H213A:3HB6H enzyme in the presence of 3HB with oxygen. A solution of the reduced enzyme (29 μM) plus 10 mM 3HB was mixed with buffer containing various concentrations of oxygen 0.13, 0.31, 0.61, and 0.96 mM (from right to left), plus 10 mM 3HB in the stopped-flow spectrophotometer. All concentrations as described were after mixing. The reaction was performed in 100 mM sodium phosphate and 100 mM sodium sulfate (pH 8.0) at 4 °C. A, the reaction was followed by monitoring the absorbance change at 400 nm to detect formation of C4a-flavin adduct intermediates and B, at 453 nm for detecting flavin oxidation. The dotted lines are the results obtained from simulations according to Figure 10. The rate constants of each step used for the simulations are according to those indicated in Table 3, and the molar absorption coefficients used for the simulations were ε_{400} of E_{red}-3HB = 4,080 $M^{-1}cm^{-1}$, ε_{400} of E_{red}

= 4050 $M^{-1}cm^{-1}$, ε_{400} of E^{*}-C4aOO(H)-3HB = 7,520 $M^{-1}cm^{-1}$, ε_{400} of *E*-C4aOOH-3HB = 8,750 $M^{-1}cm^{-1}$, ε_{400} of E_{ox} = 8,440 $M^{-1}cm^{-1}$, ε_{452} of E_{red}-3HB = 1,160 $M^{-1}cm^{-1}$, ε_{452} of E_{red} = 1,160 $M^{-1}cm^{-1}$, ε_{452} of E^{*}-C4aOO(H)-3HB = 3,130 $M^{-1}cm^{-1}$, ε_{452} of *E*-C4aOOH-3HB = 7,440 $M^{-1}cm^{-1}$, ε_{452} of E_{ox} = 11,200 $M^{-1}cm^{-1}$. Inset in B shows a plot of the observed rate constants from the first (filled-circle line) and second kinetic phases (open-circle line) *versus* oxygen concentrations.

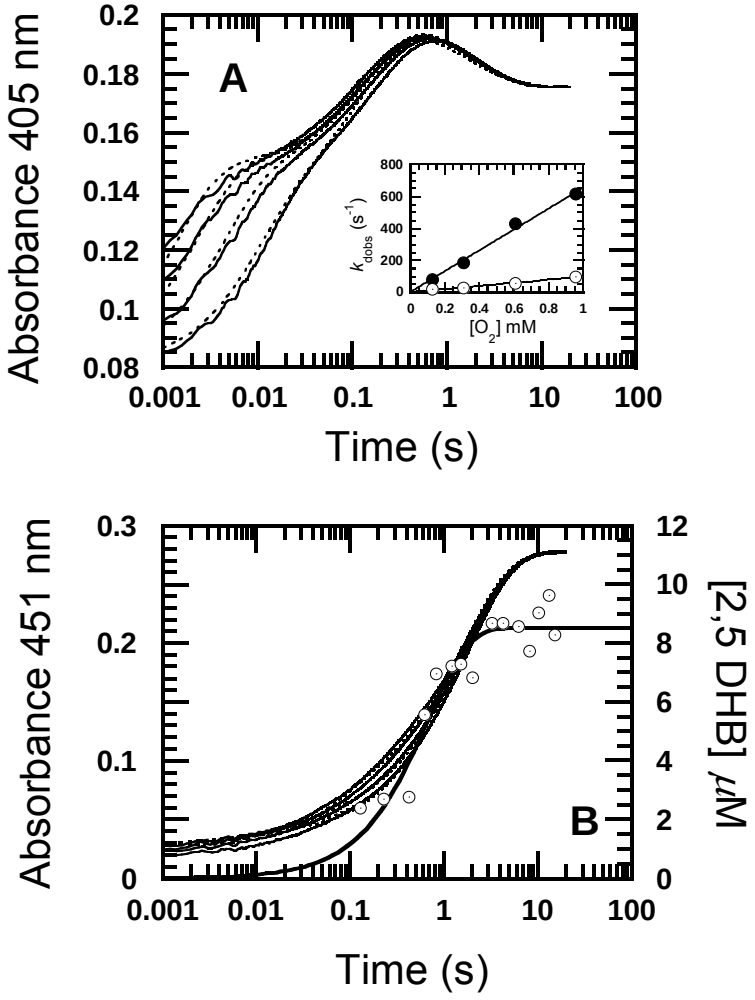

Figure 7. Reaction of reduced enzyme H213S:3HB6H in the presence of 3HB with oxygen. A solution of the reduced enzyme (25 μM) plus 10 mM 3HB was mixed with buffer containing various concentrations of oxygen of 0.13, 0.31, 0.61, and 0.96 mM (from right to left) plus 10 mM 3HB in the stopped-flow spectrophotometer. All concentrations as described were after mixing. The reaction was performed in 100 mM sodium phosphate and 100 mM sodium sulfate (pH 8.0) at 4 °C. A, the reaction was monitored by measuring the absorbance change at 405 nm to detect formation of C4a-flavin adduct intermediates and B, at 451 nm for detecting flavin oxidation. The dotted lines are from simulations according to Figure 10. The rate constants of each step used for the simulations are according to those indicated in Table 3, and the molar absorption coefficients

used for the simulations were ε_{405} of E_{red}-3HB = 3,270 $M^{-1}cm^{-1}$, ε_{405} of E'_{red}-3HB = 3,120 $M^{-1}cm^{-1}$, ε_{405} of E-C4aOO^{-} = 6,060 $M^{-1}cm^{-1}$, ε_{405} of E-C4aOOH = 8,330 $M^{-1}cm^{-1}$, ε_{405} of E-C4aOH = 8,390 $M^{-1}cm^{-1}$, ε_{405} of E_{ox} = 7,120 $M^{-1}cm^{-1}$, ε_{451} of E_{red} = 1,120 $M^{-1}cm^{-1}$, ε_{451} of E'_{red}-3HB = 1,110 $M^{-1}cm^{-1}$, ε_{451} of E-C4aOO^{-} = 1,300 $M^{-1}cm^{-1}$, ε_{451} of E-C4aOOH = 1370 $M^{-1}cm^{-1}$, ε_{451} of E-C4aOH = 1,390 $M^{-1}cm^{-1}$, ε_{451} of E_{ox} = 11,290 $M^{-1}cm^{-1}$. Inset in A shows a plot of the observed rate constants from the first (filled-circle line) and second kinetic phases (open-circle line) *versus* oxygen concentrations. Inset in A shows a plot of the observed rate constants from the first (closed-circle line) and second kinetic phases (open-circle line) *versus* oxygen concentrations. The opened-circle line in B shows a plot of product formation (at 0.13 mM oxygen) *versus* time, obtained from rapid quench-flow experiments under the same conditions as those in the stopped-flow experiments.

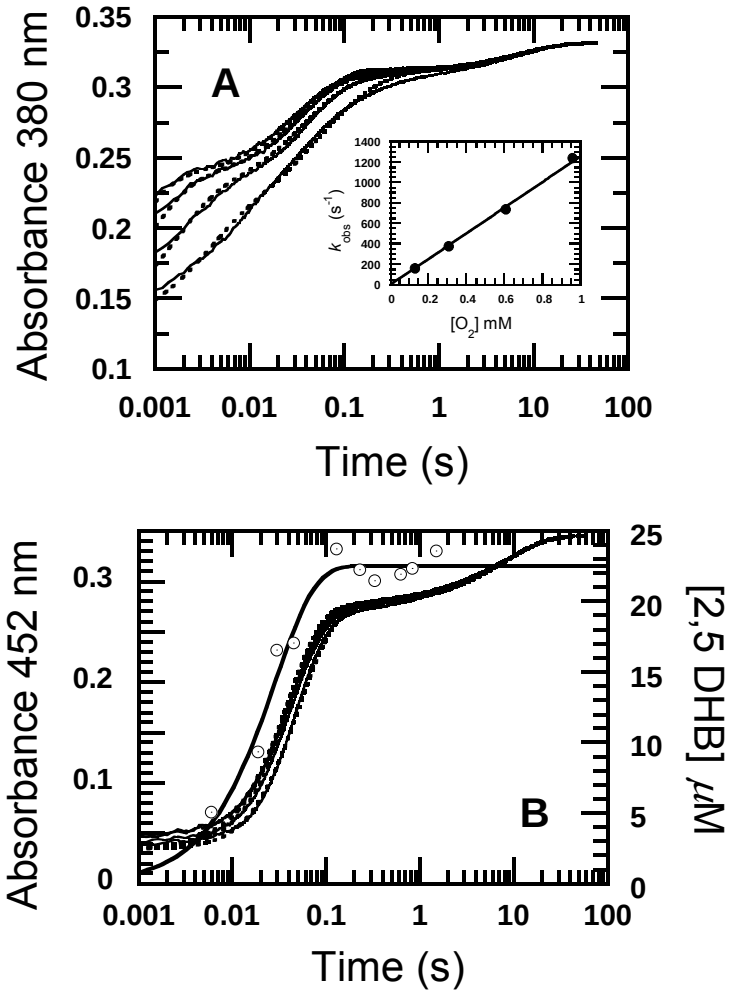

Figure 8. Reaction of reduced enzyme H213E:3HB6H in the presence of 3HB with oxygen. A solution of the reduced enzyme (29 μM) plus 10 mM 3HB was mixed with buffer containing various concentrations of oxygen of 0.13, 0.31, 0.61, and 0.96 mM (from right to left) plus 10 mM 3HB in the stopped-flow spectrophotometer. All concentrations as described were after mixing. The reaction was performed in 100 mM sodium phosphate and 100 mM sodium sulfate (pH 8.0) at 4 °C. A, the reaction was monitored by measuring the absorbance change at 380 nm to detect formation of the C4a-flavin adduct intermediates and B, at 452 nm for detecting flavin oxidation. The dotted lines are from simulations according to Figure 10. The rate constants of each step used

for the simulations are according to those indicated in Table 3, and the molar absorption coefficients used for the simulations were ε_{380} of E_{red}-3HB = 4,700 $M^{-1}cm^{-1}$, ε_{380} of E_{red} = 2,400 $M^{-1}cm^{-1}$, ε_{380} of *E*-C4aOO^{-} = 8,820 $M^{-1}cm^{-1}$, ε_{380} of *E*-C4aOOH = 9,060 $M^{-1}cm^{-1}$, ε_{380} of E_{ox}^{*} = 10,730 $M^{-1}cm^{-1}$, ε_{380} of E_{ox} = 11,520 $M^{-1}cm^{-1}$, ε_{451} of E_{red}-3HB = 1,300 $M^{-1}cm^{-1}$, ε_{451} of *E* = 1,300 $M^{-1}cm^{-1}$, ε_{451} of *E*-C4aOO^{-} = 1,200 $M^{-1}cm^{-1}$, ε_{451} of *E*-C4aOOH = 2200 $M^{-1}cm^{-1}$, ε_{451} of E_{ox}^{*} = 9,720 $M^{-1}cm^{-1}$, ε_{451} of E_{ox} = 12,000 $M^{-1}cm^{-1}$. Inset in A shows a plot of the observed rate constants from the first kinetic phase (filled-circle line) *versus* oxygen concentrations. The opened-circle line in B shows a plot of product formation (at 0.13 mM oxygen) *versus* time, obtained from rapid quench-flow experiments under the same conditions as those in the stopped-flow experiment.

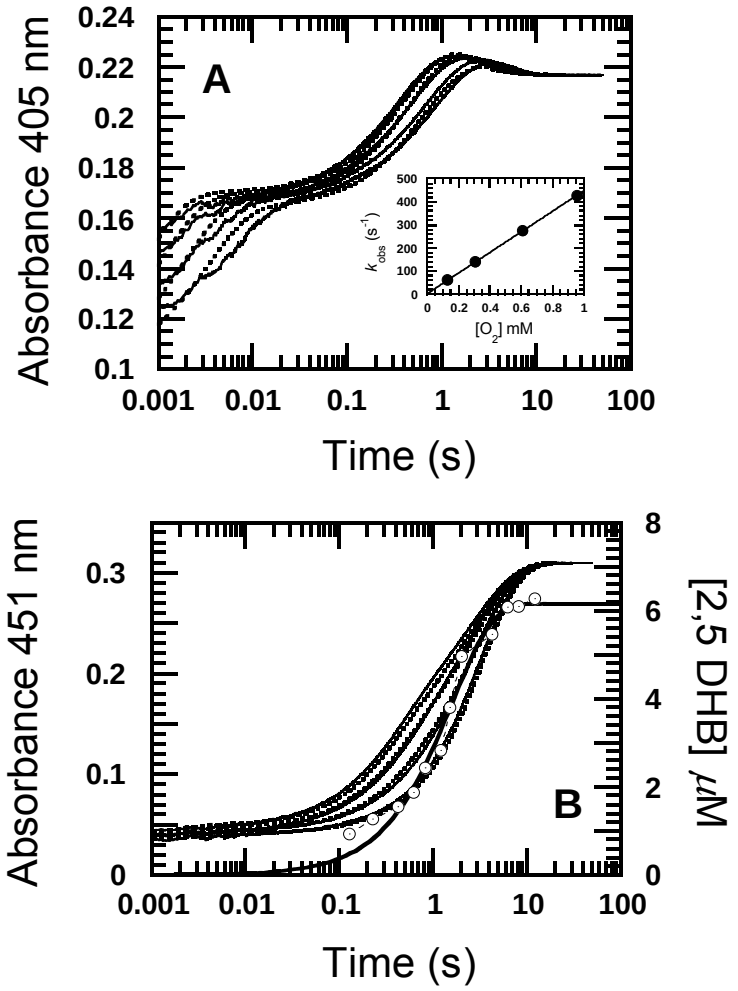

Figure 9. Reaction of reduced enzyme H213D:3HB6H in the presence of 3HB. A solution of the reduced enzyme (28 μM) plus 10 mM 3HB was mixed with buffer containing various concentrations of oxygen of 0.13, 0.31, 0.61, and 0.96 mM plus 10 mM 3HB in the stopped-flow spectrophotometer. All concentrations as described were after mixing. The reaction was performed in 100 mM sodium phosphate and 100 mM sodium sulfate (pH 8.0) at 4 °C. A, the reaction was monitored by absorbance change at 405 nm to detect formation of C4a-flavin adduct intermediates and B, at 451 nm for detecting flavin oxidation. The lower to upper kinetic traces at 405 nm and the right to left kinetic traces at 452 nm correspond to increasing oxygen concentrations. The dotted lines are from simulations according to Figure 10. The rate constants of each step used for

simulations are according to those indicated in Table 3, and the molar absorption coefficients used for the simulations were ε_{405} of E_{red}-3HB = 3,700 $M^{-1}cm^{-1}$, ε_{405} of E'_{red}-3HB = 6,190 $M^{-1}cm^{-1}$, ε_{405} of E^*-C4aOO(H)-3HB = 6,760 $M^{-1}cm^{-1}$, ε_{405} of *E*-C4aOOH-3HB = 8,340 $M^{-1}cm^{-1}$, ε_{405} of *E*-C4aOH-DHB = 8,430 $M^{-1}cm^{-1}$, ε_{405} of E_{ox} = 7,560 $M^{-1}cm^{-1}$, ε_{451} of E_{red}-3HB = 1,350 $M^{-1}cm^{-1}$, ε_{451} of E'_{red}-3HB = 820 $M^{-1}cm^{-1}$, ε_{451} of E^*-C4aOO(H)-3HB = 2,150 $M^{-1}cm^{-1}$, ε_{451} of *E*-C4aOOH-3HB = 4,200 $M^{-1}cm^{-1}$, ε_{451} of *E*-C4aOH-DHB = 2,600 $M^{-1}cm^{-1}$, ε_{451} of E_{ox} = 11,000 $M^{-1}cm^{-1}$. Inset in A shows a plot of the observed rate constants from the first kinetic phases (filled-circle line) *versus* oxygen concentrations. The open-circle line in B shows a plot of product formed at 0.13 mM oxygen *versus* time obtained from rapid quench-flow experiments under the same conditions as those in the stopped-flow experiment.

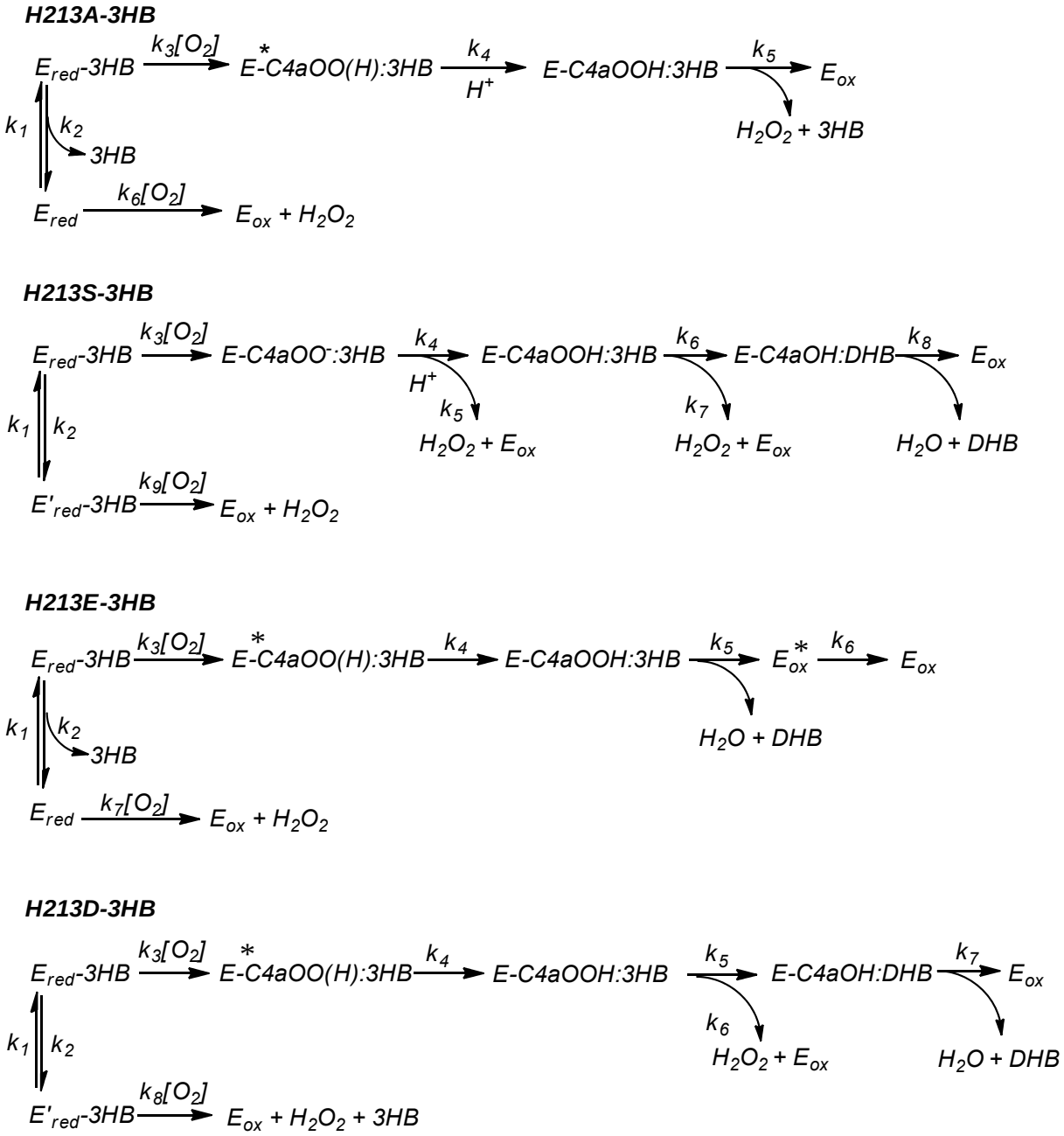

Figure 10. Proposed kinetic mechanisms for the reactions of the reduced His213 variant-3HB complexes with oxygen. The asterisks are implicated for the different conformations of *E*-C4a-OOH* changing to be fully active *E-C4a-OOH* intermediate for hydroxylation.

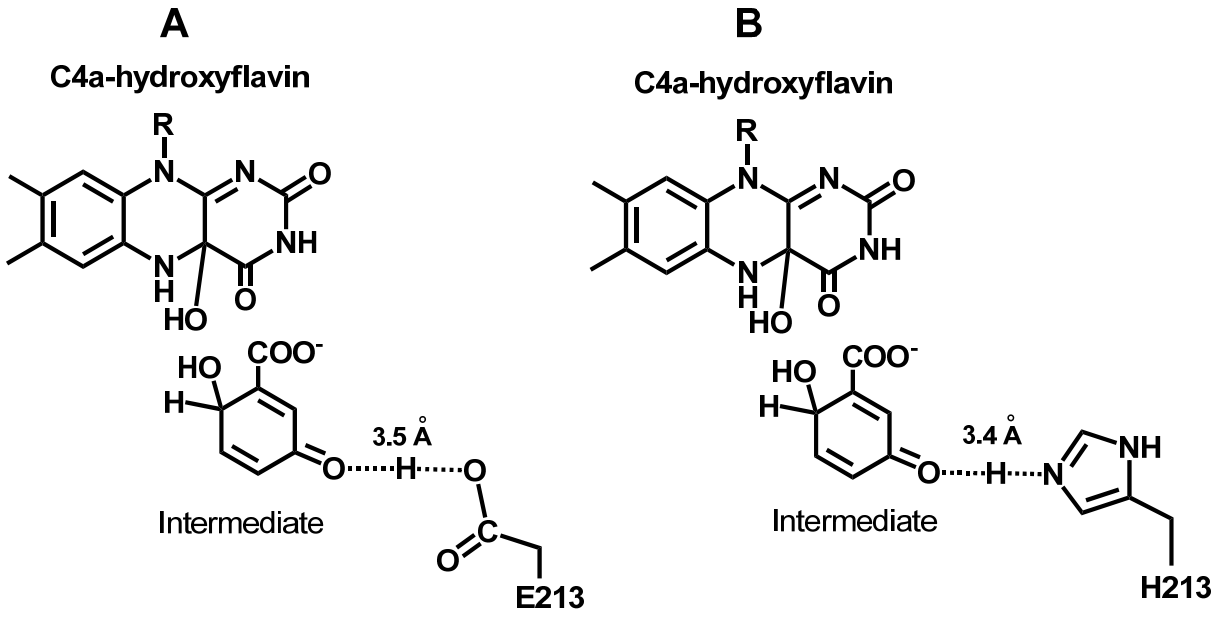

Figure 11. Proposed reaction mechanism for hydroxylation by H213E and wild-type 3HB6H. A, hydroxylation catalyzed by H213E. The carboxylate group of Glu213 acts as a catalytic base for deprotonation of the 3-OH group of 3HB to facilitate an electrophilic aromatic substitution to form a cyclohexadienone intermediate. B, in analogy to the reaction of the H213E variant, His213 is also proposed to act as a catalytic base in wild-type 3HB6H. Based on the crystal structure of the H213S variant with 3HB bound (11), *in silico* mutation of Ser213 to Glu or His shows the distance between the 3-OH group of 3HB and Glu213 or His213 as 3.5 Å and 3.4 Å, respectively.

Output จากโครงการวิจัยที่ได้รับทุนจาก สกว.

1. ผลงานตีพิมพ์ในวารสารวิชาการนานาชาติ

1.1 **Published:** Sucharitakul J, Tongsook C, Pakotiprapha D, van Berkel WJ & Chaiyen P (2013) The reaction kinetics of 3-hydroxybenzoate 6-hydroxylase from *Rhodococcus jostii* RHA1 provide an understanding of the para-hydroxylation enzyme catalytic cycle. J. Biol. Chem. 288, 35210-35221.

1.2 **Published:** Sucharitakul J, Tinikul R, Chaiyen P (2014). Mechanisms of reduced flavin transfer in the two-component flavin-dependent monooxygenases. Arch. Biochem. Biophys. 555-556C, 33-46.

1.3 Submitted: Jeerus Sucharitakul, Dheeradhach Medhanavyn, Danaya Pakotiprapha, Willem J. H. van Berkel and Pimchai Chaiyen. Tyr217 and His213 are important for substrate binding and hydroxylation of 3-hydroxybenzoate 6-hydroxylase from *Rhodococcus jostii* RHA1

2. การนำผลงานวิจัยไปใช้ประโยชน์

เชิงวิชาการ มีการพัฒนาการเรียนการสอน โดยนำกระบวนการวิธีวิจัยเสริมการเรียนการสอน เช่น การใช้เทคนิคทาง spectrophotometer ในการทำ protein-ligand binding และงานวิจัยบางส่วนเป็นวิทยานิพนธ์ระดับปริญญาโท

3. การเสนอผลงานในที่ประชุมวิชาการระดับนานาชาติ

3.1 การประชุมนานาชาติ Enzyme Engineering XXII: Emerging Topics in Enzyme Engineering ในหัวข้อเรื่อง “The Reaction Kinetics of 3-Hydroxybenzoate 6-Hydroxylase from Rhodoccocus jostii RHA1 Provide an Understanding of the para-Hydroxylation Enzyme Catalytic Cycle” 22- 26 September, 2013, Toyama prefectural University, Toyama Japan

3.2 การประชุมนานาชาติ 18th International Symposium on Flavins and Flavoproteins July 27 – August 1, 2014 The Regent Cha-Am Beach Resorts, Phetchaburi, Thailand ในหัวข้อเรื่อง “The catalytic mechanism of 3-hydroxybenzoate 6-hydroxylase from *Rhodococcus jostii* RHA1 and functional roles of active site residues”